

POLITECNICO DI TORINO

Electrical Engineering Collegio

Master course in Electrical Engineering

Master's Degree Thesis

**Sensorless Control of
Brushless DC Motor Drives**



Supervisor: Prof. Radu Iustin Bojoi

Company Tutor: Alessandro Berruti

Candidate: Matteo Notarnicola

Index

Introduction.....	1
1. Brushless DC motor drives.....	2
1.1. The Brushless motor.....	2
1.1.1. Electrical and Magnetic Model	2
1.1.2. Commutation analysis	4
1.2. Control scheme.....	6
1.2.1. Machine Control (Torque control).....	7
1.2.2. Speed control.....	8
1.2.3. Sensorless control.....	9
2. Brushless Control Board.....	11
2.1. Hardware	11
2.2. Previous Operating Status	13
3. Experimental implementation.....	15
3.1. Preliminary work.....	15
3.2. Simulation	18
3.3. Brake bench implementation.....	20
3.4. Fixed-point implementation	21
3.5. Open Loop.....	22
3.6. Current Loop	25
3.7. Speed Loop.....	29
3.8. Sensorless control.....	33
4. Future developments.....	42
Conclusions	44
Figure index	45
References	47
Acknowledgments.....	48

Introduction

The objective of this thesis is the practical implementation of classic control scheme for a Brushless DC motor. The motor is controlled through a board owned and developed by EMA srl, the work has been carried out at the company in 6 months where the project has been developed, with attention to study, verification and experimental results analysis of the phenomenon involved.

Brushless motors are a growing technology that is used to replace old, less performing DC motors. Their structure is based on a three-phase synchronous stator with a rotating magnetic field supplied by the stator windings and permanent magnets hooked to the rotor structure. From a modelling perspective, it is similar to a DC motor, having a linear relationship between current and torque, voltage and speed. While concerning its operation, the brush-system/commutator assembly is replaced by an intelligent electronic controller, which performs the same power distribution as a brushed DC motor. BLDC motors have many advantages over brushed DC motors and induction motors, such as a better speed versus torque characteristics, high dynamic response, high efficiency and reliability, long operating life, noiseless operation, higher speed ranges, and reduction of electromagnetic interference (EMI). In addition, the ratio of delivered torque to the size of the motor is higher, making it useful in applications where space and weight are critical factors. As a matter of fact, they are more often preferred to other kind of motors in industrial applications, from medium (fans, cooling systems, pumps) to very high-speed drive (spindle applications), in low power actuation (applications previously driven by DC motors) as well as in traction for hybrid electric vehicles (regenerative braking and energy recovery).

The board developed by EMA aims to support a flexible architecture for controlling Brushless motors and possibly other type of motors too. It presents: an analog-to-digital interface to acquire signals from external sources, a microcontroller to process inputs and generate command logics and a power electronics stage with driver and three-phase MOSFET inverter that provides supply to the motor. All of this is mounted on a PCB in order to achieve compactness and allow easy testing and debugging operations. The system is complete with a suite software also developed by EMA that allows to handle different features of the board such as input command via serial connection, debugging tools, error management and other.

The work has been carried out as follows:

- study on the board, determination of hardware structure and performances, analysis of the previous operating status;
- preliminary considerations, setup of the main settings like PWM signal, signal conditioning, sector definition, duty cycle computation and signal transition from the microprocessor to the power stage (gate command);
- brake bench construction, design and prototyping of a braking structure for variable load performances analysis;
- open loop, V/Hz control, starting point for diagnosis of the correctness of sector definition (position definition), current sampling, speed calculation and signal conditioning for sensorless operations;
- current loop, PI scheme tuning and implementation of a strategy for constant torque operations;
- speed loop, PI scheme tuning and digital filtering, implementation of a strategy for constant speed, load insensitive operations;
- sensorless, study of different position estimation methods and implementation of a feasible logic for open loop, constant current and constant speed operations.

The steps just described are preceded by theoretical analysis and evaluation on the expected achievements and followed by experimental results taken with EMA's instrumentation. A parallel study has been made with a MATLAB and Simulink simulation of the whole system, from the motor electrical and mechanical model to the power electronics stage and control logic implementation. The results are compared, considering the limits of each analysis and conclusions have been drawn consequently.

The thesis is concluded with an overview on the possible solutions for improving the board performances in terms of power capabilities, signal processing and flexibility of the system. This work will be helpful for future update of the hardware framework and software improvements necessary to the control technique and user interface offered by the suite.

1. Brushless DC motor drives

The term Brushless refers to an electrical drive with position feedback. So, when talking of BL drive we refer to the whole system composed by a synchronous motor, its power electronics and signal management system and its mechanical load. By extension however, the term Brushless motor is used for a three-phase synchronous motor with permanent magnet and it is called DC when it presents trapezoidal back EMF and AC when sinusoidal ones. For the same reason the motors are controlled with different techniques which will be called trapezoidal and sinusoidal for analogy with the structure of the motors.

1.1. The Brushless motor

As previously said the motor structure is composed of two main parts:

- the stator which contains the windings, they have 3-phase distribution and they generate the rotating magnetic field,
- the rotor, it hosts the permanent magnet and allows them to follow freely the stator magnetic field.

The success of this motor dwells in its features which, compared to the ones of the DC motor, make clear why always more applications now prefer the former to the latter.

One of the advantages of the Brushless motor is the absence of a commutator, main part of the DC motor, which strongly limits the max speed, the possibility of overloading the machine and gives great problems of life and reliability. Another important aspect is that the windings are in the external part, which is easier to cool down, while in the DC motor the heat generation was made on the rotor windings creating the problem of an effective heat dissipation. Finally, the use of the magnets better exploits the motor volumes, therefore the BL motor will have higher torque density, lower inertia and a better dynamic response. The only drawback in the use of a BL drive is the necessity of conversion stage made by a three-phase inverter which takes charge of the commutation role previously done by the commutator inside the DC motor structure.

1.1.1. Electrical and Magnetic Model

Based on the previous considerations the electrical and magnetic model of the motor will be analysed, a few assumptions are made to reduce the mathematical complexity of the brushless DC motor drive. They are:

- symmetrical three-phase winding,
- no magnetic saturation,
- no hysteresis and eddy current losses,
- uniform air-gap,
- armature reaction is ignored.

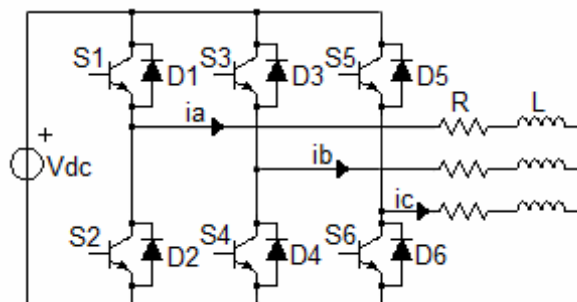


Figure 1: Electrical circuit for generic three-phase power conversion stage and electric motor

Mathematical model of armature winding, based on the circuital structure showed in Figure 1, is:

$$\begin{aligned} V_a &= i_a \cdot R + \frac{d\lambda_a}{dt} & V_b &= i_b \cdot R + \frac{d\lambda_b}{dt} & V_c &= i_c \cdot R + \frac{d\lambda_c}{dt} \\ \lambda_a &= L_{eq}i_a + \lambda_{am}(\theta) & \lambda_b &= L_{eq}i_b + \lambda_{bm}(\theta) & \lambda_c &= L_{eq}i_c + \lambda_{cm}(\theta) \end{aligned}$$

Where:

- V_a, V_b, V_c - terminal voltages of phase a, b, c [V],
- i_a, i_b, i_c - stator current of phase a, b, c [A],
- $\lambda_a, \lambda_b, \lambda_c$ - magnetic flux of phases a, b, c [Wb],
- e_a, e_b, e_c - back EMF of phase a, b, c [V],
- λ_m - permanent magnet flux [Wb],
- L_{eq}, R - per phase armature equivalent inductance [H] and armature resistance [Ω].

The electrical equations are banally obtained, while the magnetic equations need more attention. As a matter of fact, they are the ones that describe the motor typology showing the coupling between motor's magnetic fluxes. For the determination of the variable L_{eq} it is necessary to make a step back and write the magnetic equations as follows:

$$\lambda_a = L_\sigma i_a + L i_a + M i_b + M i_c + \lambda_{am}(\theta)$$

Where L_σ is the leakage inductance, L the auto-inductance and M the mutual-inductance which is equal for phase b and c given the symmetry of the windings previously mentioned.

Then considering the star without neutral winding of the phases ($i_a + i_b + i_c = 0$) the result is:

$$\lambda_a = (L_\sigma + L - M)i_a + \lambda_{am}(\theta)$$

Another important aspect is the shape of magnets and windings distribution, they both influence the production of back EMF. The objective is to have squared induction and a uniform distribution of stator windings. In fact, the magnetic flux is the results of the integral of the product between the magnet induction and the square of the conductor distribution, while the phase EMF is the derivate of the same flux, which is the one wave that has to be trapezoidal.

Substituting the variable λ obtained from the magnetic equation in the electrical equation the result is the following:

$$V_a = i_a \cdot R + L_{eq} \frac{di_a}{dt} + e_a \quad V_b = i_b \cdot R + L_{eq} \frac{di_b}{dt} + e_b \quad V_c = i_c \cdot R + L_{eq} \frac{di_c}{dt} + e_c$$

Where:

$$e_a = \frac{d\lambda_m}{dt} = \frac{d\lambda_m}{d\theta} p \omega_m$$

Operating the energy balance trough multiplying voltage and current it is possible to analyse how the power contribution are divided, the calculation is made only on one phase for shortness:

$$V_a i_a = R i_a^2 + i_a L_{eq} \frac{di_a}{dt} + e_a i_a$$

The total of each value will be given by summarizing the contribution of the three different phases. The input electrical power corresponds with the product $V_a i_a$, the value $R i_a^2$ represents the Joule dissipation through thermic energy, the product $i_a L_{eq} \frac{di_a}{dt}$ stands for magnetizing power and finally the product $e_a i_a$ represents the mechanical power for torque generation. Considering the relationship that links mechanical power and torque it is possible to obtain the torque equation for the BLDC motor:

$$T_e = \frac{e_a i_a + e_b i_b + e_c i_c}{\omega_m}$$

Which, considering $e_a = \frac{d\lambda_m}{d\theta} p \omega_m$, can also be expressed like:

$$T = p \left(i_a \frac{d\lambda_{am}}{d\vartheta} + i_b \frac{d\lambda_{bm}}{d\vartheta} + i_c \frac{d\lambda_{cm}}{d\vartheta} \right)$$

Is important to notice that the presence of the pole pairs value in the equation does not mean that the torque is directly proportional to this number, given that is valid the relationship:

$$\frac{d\lambda_{im}}{d\vartheta} \propto \frac{1}{p}$$

Which ensures the absence of dependency between torque and pole pairs number.

The torque relation as previously written is not linked to the particular structure of the motor so it is valid for trapezoidal and sinusoidal motors alike. The variation is introduced when considering the particular waveform of the magnet flux λ_m .

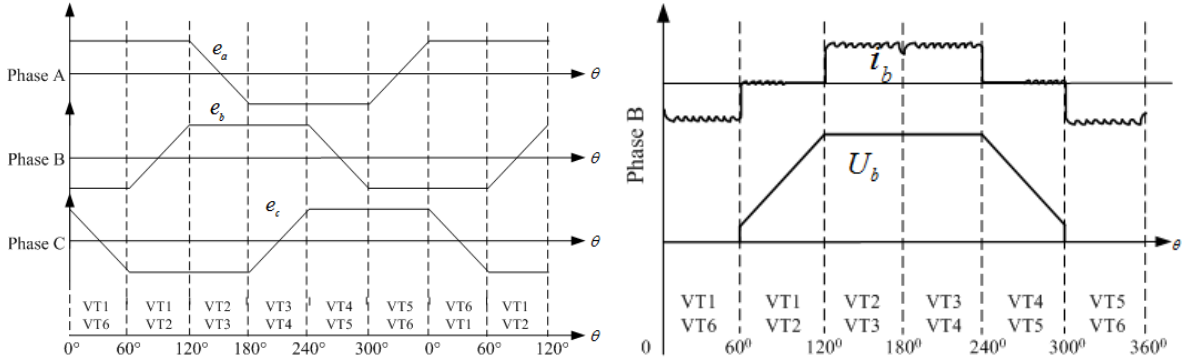


Figure 2: Back EMF waveforms for BLDC motor and sector partitioning (left), current waveform and phase relation with the same phase BEMF (right)

Considering trapezoidal waveform, the air gap circumference will be divided in 6 sectors as shown in Figure 2, consequently the torque equation, which is general, takes the following form:

$$T_e = \frac{2e_p i_p}{\omega_m}$$

Where: e_p - phase back EMF [V], i_p - non-zero phase current [A].

All the torque formulations provide one important information about how to control BL motors, both with trapezoidal or sinusoidal technique, in order to have a positive torque the sum of the products $e_p i_p$ must be positive, which becomes easier for the BLDC considering one of the three members of the product is always zero.

1.1.2. Commutation analysis

The commutation stage is a fundamental part of the behaviour of a motor, moreover for the BLDC motor where the transition of the phases command needs to be smoother and controlled as possible to ensure the perfect functioning of the drive operation, both in dynamic and regime evolution. The studio of the phenomenon is brought on by obtaining the equations that describe the aspect of this stage and then analysing how it is possible to play with them in order to develop different results and performances.

The BLDC motor needs only two phases conducting and creating current in order to produce a constant flat torque, while the sinusoidal technique needs always three active phases in order to create sinusoidal waveforms and respect the equation $i_a + i_b + i_c = 0$.

Even if talking of the BLDC the three-phase-on strategy needs to be considered given that the switching phenomenon involves all the three phases and, when incomplete, can involve also the third non-conducting phase. To analyse this situation the currents i_a and i_b will be used as state variables, starting from the calculation of the phase-to-phase voltage during the transition from a-c to b-c conduction:

$$v_{ac} = R(2i_a + i_b) + L_{eq} \left(2 \frac{di_a}{dt} + \frac{di_b}{dt} \right) + e_{ac} \quad v_{bc} = R(i_a + 2i_b) + L_{eq} \left(\frac{di_a}{dt} + 2 \frac{di_b}{dt} \right) + e_{bc}$$

It is possible to neglect the resistance R and then obtain the state equation for the three-phase-on:

$$\frac{di_a}{dt} \cong \frac{(2v_{ac}-v_{bc})-(2e_{ac}-e_{bc})}{3L_{eq}} \quad \frac{di_b}{dt} \cong \frac{(2v_{bc}-v_{ac})-(2e_{bc}-e_{ac})}{3L_{eq}}$$

These equations describe the dynamic evolution of the two currents the third current stays flat but, considering that $i_a + i_b + i_c = 0$, they can describe its trend when the equality of the derivatives is not observed.

The two-phase-on state is more easily described by the equation:

$$\frac{di_b}{dt} \cong \frac{v_{bc} - e_{bc}}{2L_{eq}}$$

Which is calculated considering only phase b and c are conducting.

In order to have a better perception of the situation, the voltage phase regulation will be neglected and will be studied the evolution of the events when working with a six-step control.

The six-step strategy is a borderline operation where the stator voltage is not modulated. Its use involves lack of control on the stator voltage and current, current ripple and torque ripple but, even if its not a very performance way of controlling the motor, its study is important to analyse the state parameters behaviour during the commutation between the different sectors of the motor circumference.

The reference equations to study the commutation event are the previously mentioned three-phase-on state equations. For this situation it is possible to determine the values of the voltages involved. Immediately after the commutation the voltage $v_{13} = 0$, while v_{23} will be set to the DC link voltage value, the EMF e_{13} and e_{23} are both equal to $2E(\omega)$ (the statement is true for e_{23} , while for e_{13} just as a first approximation), thus determining the state equations:

$$\frac{di_a}{dt} \cong \frac{(-V_{DC})-2E(\omega)}{3L_{eq}} \quad \frac{di_b}{dt} \cong \frac{2V_{DC}-2E(\omega)}{3L_{eq}}$$

The condition for a complete commutation is expressed by the relationship $\frac{di_a}{dt} = -\frac{di_b}{dt}$ which is verified when $V_{DC} = 4E(\omega)$. This condition means the necessity of a voltage regulated DC-link which is impractical and not used. Considering the EMF variability because of the rotor speed, when using six-step control is acceptable to have incomplete commutation, is one its main drawbacks. But when is not acceptable to have torque ripple and lack of control on the current evolution, consequences of an incomplete commutation, it is necessary to regulate the stator voltage controlling the inverter leg status at high frequency with a PWM logic.

A Pulse-Width Modulation allows to adjust the voltage fed to the windings and follow the current evolution reducing loss of control on its evolution. To ensure that the commutation is completed is necessary to respect the condition $\frac{di_a}{dt} = -\frac{di_b}{dt}$, which means:

$$v_{ac} + v_{bc} = 4E(\omega)$$

The solution to this relationship is not univocal and depends on the modulation technique chosen. Breaking up the addend it is possible to see the elements involved: $v_a - v_c + v_b - v_c = 4E(\omega)$. The value of v_a is zero given that the phase is opening, so the remaining voltages need to be determined to complete the equation.

If the modulation technique implemented follows the condition $v_c + v_b = 0$, the result is that $v_b = -v_c = \frac{4E(\omega)}{3}$. In order to respect the previous equation one modulating signal and two carrier waves are needed, the effect is two complementary gate commands that impose a phase-to-phase voltage with two-level variability and a ripple with same frequency of the carrier waves frequency. The outcome for the conduction regime will be the one in Figure 3 (left), the figure shows the implementation of a Bipolar control scheme for a sinusoidal wave, but the effects can be easily extended to BLDC motor control.

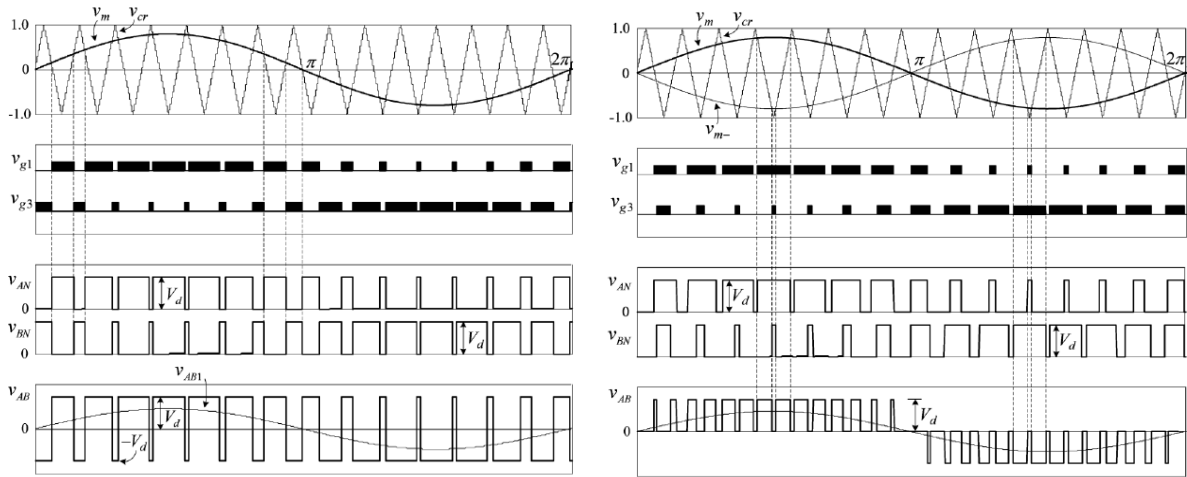


Figure 3: Waveforms of modulation scheme, Bipolar (left), Unipolar (right). From top to bottom: carrier wave and modulating signal, gate command voltages, phase voltages, phase-to-phase voltage and moving average

It is possible to complete the equation also by not respecting the condition $v_c + v_b = 0$, in this case a Unipolar control scheme will be adopted and only one out of three inverter legs will be controlled during the switching operations. So, with $v_a = 0$, $v_b = V_{DC}$, to rapidly lead the current to its regime value, v_c will be $\frac{V_{DC} - 4E(\omega)}{2}$ which is valid only in a limited range of voltages (speed), given that v_c can vary only between 0 and V_{DC} .

The effects during the conduction regime are shown in Figure 3 (right): using only one carrier wave and two complementary modulating signals the results are three-level phase-to-phase voltages and a current ripple reduced in amplitude thanks to the frequency twice the frequency of the carrier wave.

The use of a Unipolar strategy has implication in the machine control which will be later explained.

1.2. Control scheme

The review focuses now on how the motor parameters are managed in order to obtain electromechanical conversion and therefor torque production. In Figure 4 is shown the most general block diagram for a position control of a BLDC motor. By leaving out parts of this scheme is possible to obtain different control loop depending on what is requested to the motor.

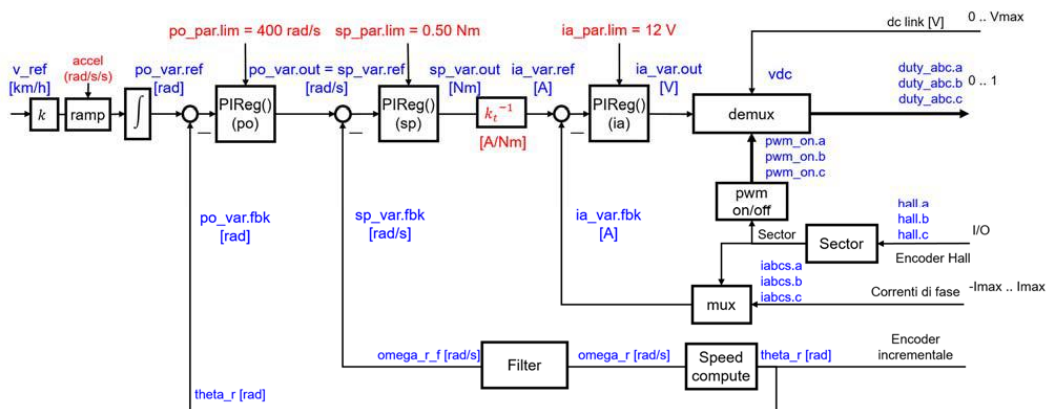


Figure 4: Block diagram for BLDC drive control, general configuration of a position control and focus on the digital control part of the scheme

1.2.1. Machine Control (Torque control)

The machine control is the first aspect that needs to be addressed in order to properly move each kind of motor. It involves motor mechanics, its electrical and magnetic model, currents management and the transition between the analog and digital worlds, in both directions. The analysis will be conducted on a Unipolar control technique implemented on a BLDC motor.

The main implication of using a BLDC motor is the presence of trapezoidal back EMF waveforms, they are very useful in helping determine the rotor position given that they divide the air gap circumference in 6 angular sectors which are easily observed using 3 hall effect sensors spaced by 120 electrical degrees. Following the considerations preciously made, the unipolar strategy implies the control of one stator current at a time and two phase voltages.

The block diagram in Figure 5 shows the graphic implementation of this process:

- The currents are measured using current sensors directly placed on the phase connections, the results will be a set of 6 currents that will be passed to the MUX block and, together with the information of the hall sensors placed on the motor, will determine two feedback currents;
- Confronting the absolute value of the currents is possible to determine the rotating direction and therefor chose the one feedback current that will be used for error calculation in the loop;
- A PI regulator, properly tuned, produces a voltage reference according to the current error that needs to be deleted;
- The voltage reference is then used to generate the three-phase commands for the inverter legs, this are compared with a single carrier wave that sets the switching frequency of the inverter and the duty cycle to apply;
- The DEMUX block takes as inputs the position information from the hall sensors and the commands, this block works both in the analog and digital world, it receives these information, choses the two phases that will conduct and sends the output to the driver that will generate the gate command for the inverter switches.

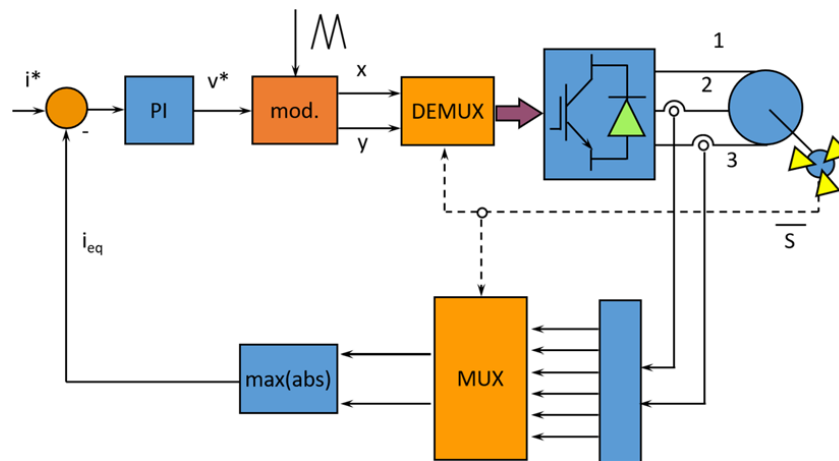


Figure 5: Machine control for BLDC motor, block diagram of the whole system: digital control, power conversion stage, motor and analogic data acquisition

The current error compensation and voltage reference generation of the torque loop of a BLDC makes understand why the drive uses the acronym DC even if it is supplied by three phase voltages. In a sinusoidal drive in fact there would have been three different feedback currents and three references to generate the commands (in a fixed axis control), the presence of trapezoidal back EMF and the use of hall effect sensors allows a scalar control and a great simplification for the computing components.

The machine control is a loop customized on the kind of motor to be controlled and its constructive aspects. Considering the analogy with the DC motor, the torque control becomes a current control just by means of the torque constant k_T , this allows to use current sensors which are space-saving and cheap unlike torque sensors.

Finally, the current control needs the tuning of the PI regulator:

- The proportional part has the role of reducing as much as possible the error in regime conditions, achieving the reference as quickly as possible in the dynamic evolution, without overshooting the objective. The k_p value is calculated by the product $k_p = \omega_b \cdot 2L_S$. L_S is the stator inductance and ω_b the loop desired bandwidth.
- The integral part has the role of deleting the error caused by the additive noise in regime functioning, in a current loop the noise is given by the load torque applied to the motor. The k_I value is calculated by $k_I = \omega_b \cdot k_p$. However, this number is generally too big, so it is recommended to use 1/3 or even 1/4 of the k_I value.

The bandwidth is a crucial parameter that symbolises the performance of the control. As a matter of fact, a high bandwidth value allows to control and better reconstruct the wanted waveform, the control loop bandwidth needs to ensure this performance and create a signal with a fine resolution. But an upper limit to this value exists and it is determined by the technological limits of the conversion stage, as a matter of fact the switching frequency on the inverter's switches gives the maximum value of frequency signal it can recreate. So, a good rule to ensure fine signal reconstruction and good exploitation of the technology performances is choosing the current bandwidth as 1/10 of the switching frequency the electrical switches allow to reach, the same is valid in the determination of the speed loop bandwidth, but this will be discussed later.

1.2.2. Speed control

The speed loop is a control strategy independent by the kind of motor used, at least as a first approximation, it involves a PI regulator that produces a torque reference starting by a speed error and it uses a measured, observed or estimated speed as a feedback signal to be compared with the reference speed to be obtained.

The PI tuning is more delicate in this case, from the block diagram analysis and considering the inner current loop as a unitary gain, as done for the current loop, it is possible to determine the values of the PI gains. The k_p value is calculated as $k_p = \omega_b \cdot J_{eq}$, while the k_I value is $k_I = \omega_b \cdot k_p$. The bandwidth ω_b is a value calculated as at least 1/10 of the current loop bandwidth and the moment of inertia J_{eq} is determined considering all the mechanical parts involved. Clearly the proportional and integral gains are highly dependent on whether the motor is freely spinning, or it is moving a load, especially when the applied torque load is not so easily definable.

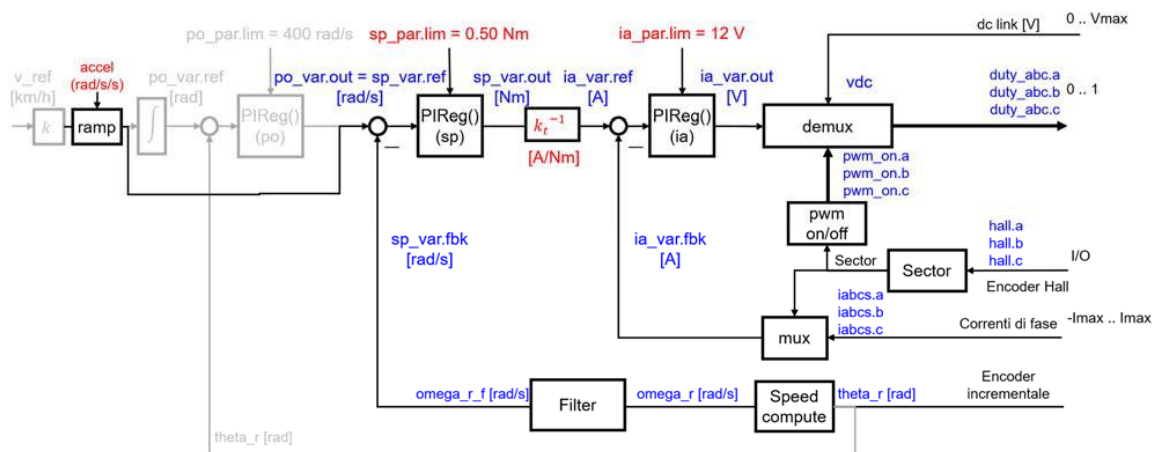


Figure 6: Speed loop control block diagram, focus on the digital control system

The diagram in Figure 6 shows a speed loop example, generally the input is a speed step with a limited acceleration which modifies the reference in a ramp command and the output is a requested torque which translates in a requested current for the inner loop.

One significant feature is how the speed is determined, position and speed sensors come in different shapes and form, so it is important to properly know them and use the right one for the requested application.

Hall effect sensors are little sensors that produce a signal when invested in magnetic field, they are perfect in applications that involve permanent magnet and that have not so much space to invest on bigger structures. The number used may vary but they are mainly used in triplets and spaced by 120 electrical degrees in BLDC motors, this is the minimum number of sensors for the sector definition, but the information can be used also to determine the rotor position and speed. In order to obtain more resolution and a more accurate measure more sensors are needed but, when the application requires it, different solutions are preferred to a higher number of hall effect sensors.

Numerous are the existing technologies used for the speed calculation, some of those are the dynamo tachometer realized with a DC motor, the brushless tachometer realized with a BLDC motor and the resolver, but one of the most used is the Encoder. It can be an absolute or an incremental Encoder and its functioning is based on a series of marks that give a discretized position information, the higher the number of marks more accurate is the position and therefore speed measure.

An effective speed loop must have a speed sensor, but its not unusual to come across motor drives that do not use any Encoder or other sensor, as a matter of fact any additional part is an extra cost and if it is possible to eliminate it, so be it. This is the stage of sensorless drives, BLDC motors can easily work even without encoder due to the presence of the hall sensors, but other motors not have other sensors on which rely. Sensorless control is different from one motor to the other, given that uses physical and mechanical features of the own machine, in general however the term is used for those applications that do not use any sensor for the speed measure, by extension the word can also be used for BLDC motors without hall effect sensors, which will be the case discussed in the next section.

1.2.3. Sensorless control

Position sensors can be completely eliminated, thus reducing further cost and size of motor assembly, in those applications in which only variable speed control (no positioning) is required and system dynamics is not particularly demanding (slowly or, at least, predictably varying load). In fact, some control methods, such as back-EMF and current sensing, provide, in most cases, enough information to estimate with sufficient precision the rotor position and, therefore, to operate the motor with synchronous phase currents.

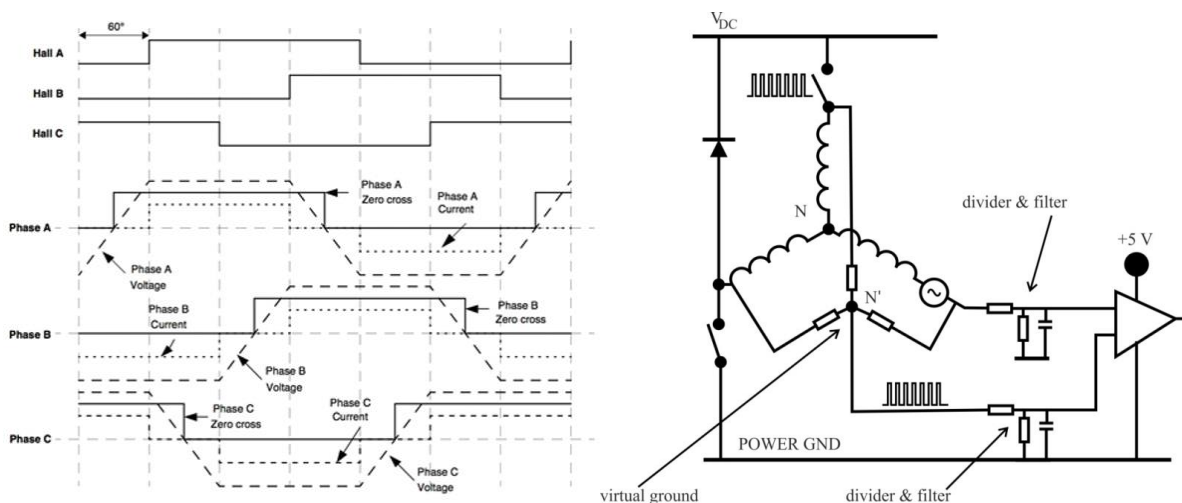


Figure 7: Zero-crossing events and comparison with hall effect sensors signal (left), comparison circuit for zero-crossing detection, division and filtering on phase voltage and virtual ground (right)

The BLDC motor provides an attractive candidate for sensorless operation, because the nature of its excitation inherently offers a low-cost way to extract rotor position information from motor-terminal voltages. In the excitation of a three-phase BLDC motor, except for the phase-commutation periods,

only two of the three phase windings are conducting at a time and the no conducting phase carries the back-EMF. There are many categories of sensorless control strategies, however the most popular category is based on back electromotive forces or back-EMFs. Sensing back-EMF of unused phase is the most cost efficient method to obtain the commutation sequence in star wound motors. Since back-EMF is zero at standstill and proportional to speed, the measured terminal voltage that has large signal-to-noise ratio cannot detect zero crossing at low speeds. That is the reason why in all back-EMF-based sensorless methods the low-speed performance is limited, and an open-loop starting strategy is required.

The zero-crossing approach is one of the simplest methods of back-EMF sensing technique and is based on detecting the instant at which the back-EMF in the unexcited phase crosses zero. The back-EMF of floating phase is sensed and its zero crossing is detected by comparing it with neutral point voltage. This scheme suffers from high common mode voltage and high frequency noise due to the PWM drive, so it requires low pass filters, and voltage dividers, as shown in Figure 7 (right). Filtering introduces commutation delay at high speeds and attenuation causes reduction in signal sensitivity at low speeds, which is why the speed range is narrowed in direct back-EMF detection methods.

For typical operation of a BLDC motor, the phase current and back-EMF should be aligned to generate constant torque. The current commutation point can be estimated by the zero-crossing point of back-EMFs and a 30° phase shift. This zero crossing triggers a timer, so that the next sequential inverter commutation occurs at the end to this timing interval. In order to produce maximum torque, the inverter should be commutated every 60° by detecting zero crossing of back-EMF on the floating coil of the motor, so that current is in phase with the back-EMF.

Three low-pass filters (LPFs) are utilized to eliminate higher harmonics in the phase terminal voltages caused by the inverter switching, but the time delay introduced by them will limit the high-speed operation capability of the BLDC machine.

An alternative to the use of analog LPFs, a Unipolar Pulse Width Modulation scheme can be used to measure terminal voltages: the true phase back-EMF signal could be directly obtained from the motor terminal voltage by properly choosing the PWM and sensing strategy. The method consists of sampling the voltage signal in a specific moment during the period of regulation imposed by the inverter switching logic. This would provide advantages such as no sensitivity to switching noise, no filtering required and good motor performance in a wide speed range.

The price for the simplicity of the zero-crossing method tends to be noise sensitivity in detecting the zero crossing, and degraded performance over wide speed ranges unless the timing interval is programmed as a function of rotor speed. Another drawback is that it is not possible to use the noisy terminal voltage to obtain a switching pattern at low speeds since back-EMF is zero at standstill and proportional to rotor speed. Also, the estimated commutation points have position error during the transient period when the speed is accelerated or decelerated rapidly, especially for a system that has low inertia.

The advantage of sensorless BLDC motor control is that the sensing part can be omitted, and thus overall costs can be considerably reduced. The disadvantages of sensorless control are higher requirements for control algorithms and more complicated electronics.

In this part only one method of controlling a sensorless BLDC motor has been discussed, as introduction to the aspect and to focus the attention on the main topic of this thesis. The next parts will show how all of the theoretical consideration until now made are integrated on the board and has been useful for the development of the final working setup. The last part instead will consider any improvement or modification to the current operating status, based on the available options, in order to allow better performances, ease for future developments and include different features possibly helpful.

2. Brushless Control Board

The board developed by EMA aims to support a flexible architecture for controlling Brushless motors and possibly other type of motors too. As a matter of fact, it presents all the features to properly drive three-phase motors: an analog-to-digital interface to acquire signals from external sources, a microcontroller to process inputs and generate command logics and a power electronics stage with driver and three-phase MOSFET inverter that provides supply to the motor. All these parts are placed on a PCB in order to achieve compactness and allow easy testing and debugging operations. Its main purpose is driving BLMs both with sensed and sensorless logic, but its characteristics allow the possibility of controlling different types of three-phase motors that fit the power capability of the electrical configuration.

The system is complete with a suite software also developed by EMA that allows to handle different features of the board such as input command via serial connection, debugging tools, error management and other. The thesis, however, is focused on the motor drive, so little attention was given to the suite software.

2.1. Hardware

In this section will be provided a view of the physical components that compose the board, they determine the electrical capabilities and limits of the system, giving an idea of what it can do and how much its performances can be enhanced.

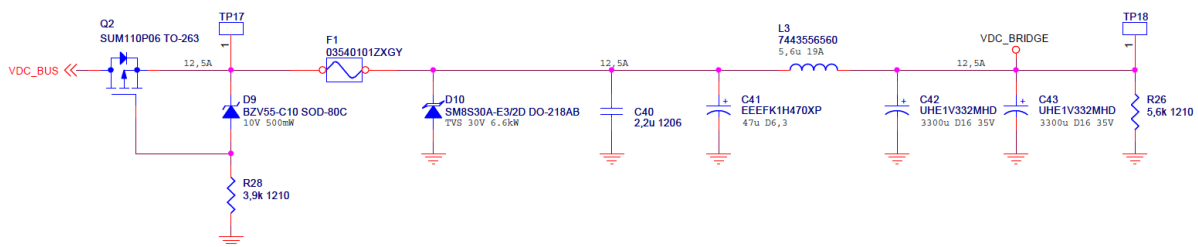


Figure 8: Supply circuit of the board, board schematic

The power input circuit schematic is shown in Figure 8, the board requests a 24 V direct current supply, it presents a fuse to ensure protection from overcurrent events and a CLC filter, which completes the DC bus, in order to dampen any fluctuation of the input voltage. System design defines the voltage working ratio between 8-30 VDC while the power connectors of the board can handle until 15 A max, which means a maximum power input of 475 W. The electronic systems requesting a different voltage are managed by an internal power supply that adapts the voltage fed to the electronic components in two levels, 3.3 and 5 V. The power output is the connection to the motor phases, as for the DC bus the connectors can handle 15 A max thus allowing to feed to the controlled motor until 475 W.

The input fed to the board, other than the voltage supply, are small signals useful for the management of the board and the motor. As a matter of fact, 5 different input allow to generate a reference speed for the board software:

- External voltage source with 4 upper and lower limits (0-5 V, 0-10 V, -5-5 V, -10-10 V),
- Analogic potentiometer,
- Push buttons for increasing and decreasing the reference,
- Externally fed square wave with duty cycle proportional to speed reference,
- UART connection for input/output communications through suite software.

The power conversion stage has a three-phase inverter structure and it is composed by 6 MOSFET, the role of free-wheeling diode is given to the internal body diode of the transistor. The max voltage the component can bear is 60 V between drain and source while the continuous current performance is 90 A of drain current with a drain-source resistance of 3.5 mΩ. As can be seen in Figure 9, every MOSFET

has its own gate circuit composed by two resistances and one diode, the gate command is fed in output by the Driver which is connected with 6 different pins to the 6 MOSFET and manages in input the signal coming from the microprocessor.

The Driver is a Digital-to-Analog interface that generates the gate voltages needed for the right power electronics operations. Citing from its own data-sheet: “It is a 3-phase controller for use with N-channel external power MOSFETs and is specifically designed for automotive applications. Full control over all six power FETs in the 3-phase bridge is provided, allowing motors to be driven with block commutation or sinusoidal excitation”.

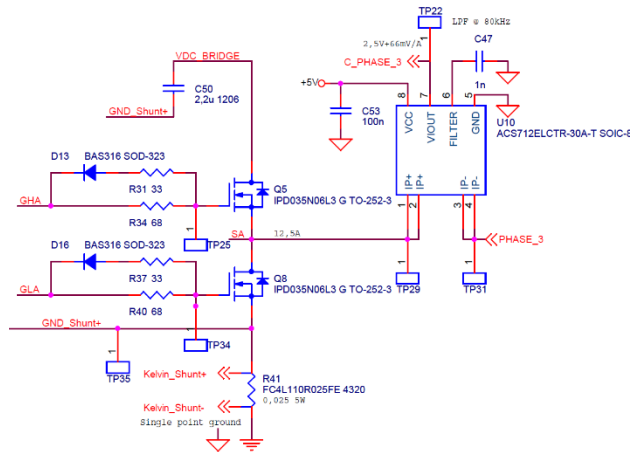


Figure 9: Board schematic for inverter leg, gate command circuit, shunt resistor and current sensor

The power conversion stage is cooled down with a forced convection mechanism, a fan mounted above the PCB aligned with the MOSFETs extracts the heat according to the feedback coming from the temperature sensors mounted below the PCB, close to the drain of the components.

The control of electrical drives relies a lot on measuring electrical and mechanical parameters by using sensors, particularly current sensors and position sensors. These signals need to be passed to the microprocessor by modifying their properties but leaving intact the information within. Again in Figure 9 it is possible to see the hall effect current sensor for one of the three inverter legs, every leg represents one motor phase, so it will have one current sensor. These ones are 30 A full-scale components with an 80 kHz bandwidth, later will be discussed why it was decided to replace these sensors with 5 A full-scale ones.

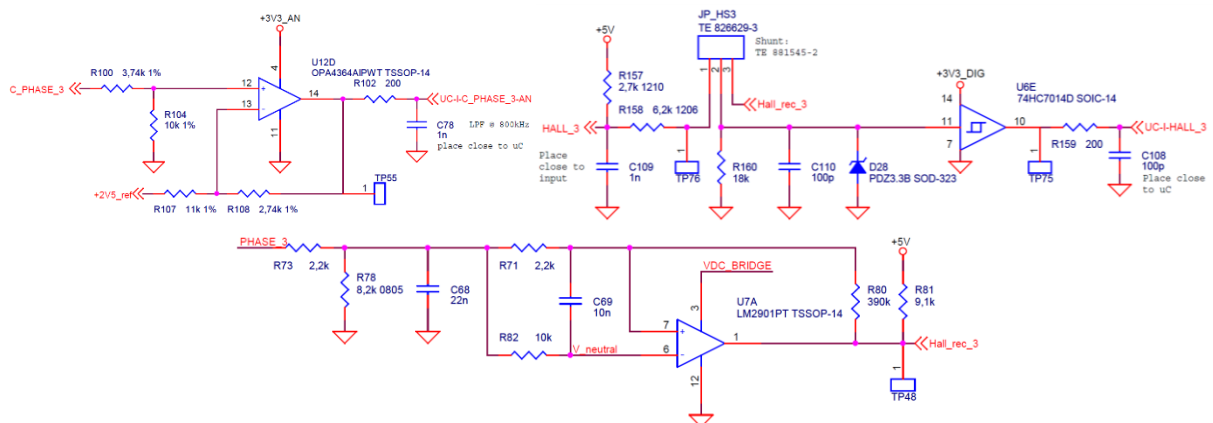


Figure 10: Board schematic for main signal conditioning: phase current (up left), hall effect sensor and jumper for selection of real or reconstructed signal (up right), reconstruction of position signal from back-EMF (down)

As previously said the board as the interface to control a motor both in sensored and sensorless mode, in Figure 10 is showed the signal conditioning of the main sensors used. The signal conditioning of the current sensors is made by a voltage divider that adapts the sensor voltage level to the 3.3 V of the processor pins and an analog low pass filter that reduces the fluctuations of the measure. The

management of the position information is made by three jumpers on the board, one for each phase: if the jumper short-circuits the terminals 1 and 2 the signal coming from the hall sensors mounted on the motor stator is reduced in magnitude with a voltage divider, then passed to a buffer and filtered with an RC filter. If the jumper short-circuits the terminals 2 and 3 the signal will be a reconstruction of the hall sensors, the phase voltage will be divided and filtered as for the other signals, then the obtained voltage will be compared to a virtual neutral point voltage obtained by using a star connection external to the stator windings, also divided and filtered. The output of the voltage comparator follows the same path inside the buffer and then the RC filter.

The brain of this application is a Digital Signal Controller by Microchip. It has 64 pins, 40 MHz clock (40 MIPS), 8 kbyte RAM, 64 kbyte Flash Memory and Timers counting on 16 or 32 bits. Considering the ultimate goal of the board, the microcontroller chosen is for electrical drive command purposes, as a matter of fact it presents a PWM Motor Control module, a Quadrature Encoder interface and other modules useful for the control of electrical motors. Finally, it presents 1 ADC module with up to 16 channels, selectable with the internal device registers. The ADC configuration can be 10-bit, 4 S&H and 1.1 Msps or 12-bit, 1 S&H and 500 ksps.

The last part of the system is the motor which is external to the board, but it is a fundamental component of the drive. The one used during the work is a 65 W, 24 VDC rated Brushless DC motor, it has 8 pole pairs, rated current and torque of 3.26 A and 0.13 Nm, max current and torque of 9.5 A and 0.39 Nm and rated and no-load speed of 4840 and 6100 rpm. Some attempts have been made with other motors and will be discussed later, but the main work relies on the just described component.

2.2. Previous Operating Status

In order to sum up the complete structure of the board and its main functioning, the system design will be quoted, next there will be a focus on other features set through the processor registers and pre-existent software.

“Purpose of the system is to control a brushless motor, the implementation is performed through an embedded firmware; it shall be fully parametric, to adapt itself (through a calibration set) to several motor types differing in size, voltage ratings, torque. Due to research purpose of the project, system can be configured in several ways: target motor speed can be set through different types of input command selectable among PWM, Voltage, UART and on-board push-buttons. If selected input is voltage, signal can be taken from an external source or, through an on-board potentiometer, generated locally from power supply. A set of jumper interfaces allow the user to set several system configurations: voltage input dynamics, hall signal source and potentiometer enabling.

System drives BLDC motors in both clockwise and counter-clockwise directions; 4 pre-defined command laws are available, 2 single wise and 2 bi-directional, selectable through jumper interface. LEDs are provided to inform the user about status of the system and abnormal situations. System shall provide other buttons for management of some critical system states.

System shall be able to drive both sensed and sensorless motors. In the former case system shall acquire 3 hall signals from relative sensors, in the latter case these signals will be internally built by hardware implementation starting from BEMF. Each motor phase is driven by a half-bridge configuration power stage, constituted by two MOSFET transistors. For each phase are necessary a high side signal and a low side signal. So, in order to drive the three motor phases, six signals are necessary for the six MOSFET gates. The microcontroller generates these six signals, but it is necessary to put a driver between microcontroller and power stage. Driver has only to adapt voltage level from 3.3V generated by microcontroller to level required on gates of power stage MOSFETs with an adequate gate current.”

The previous operating status relied on a closed loop speed control with no internal current loop, as shown in Figure 11. As a matter of fact, the ADC module was set with a sampling frequency of 25 Hz and a 12-bit configuration, which allows to have 1 S&H, so only one channel at a time is sampled. This sampling speed can not allow any kind of control over the parameters, so that the information acquired

are used only for diagnostic purposes. The signals detected by the channels are the three phases currents and voltages, the DC-link current and voltage, the virtual neutral voltage and the potentiometer voltage for the reference speed information.

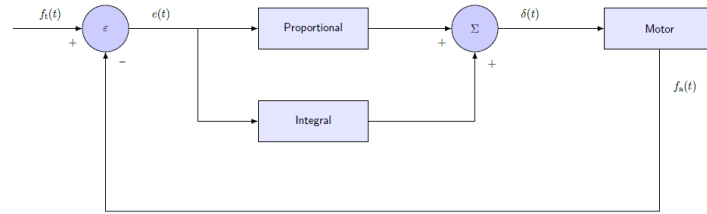


Figure 11: Speed control closed loop implemented in previous software

About the system control, the reference speed is provided by one of the previously mentioned ways and then it is compared to the feedback speed, which is estimated by calculating the time interval between the hall sensors' edges. The error resulting by the subtraction between these two terms is sent to a PI regulator, tuned separately with a Simulink block diagram. The output is a duty cycle value which is then converted to a DSP register suitable value that will be sent to the driver and then used to command the gate of the power FETs accordingly.

Even if using a scalar control technique, the voltage regulation is needed to ensure the speed error cancellation and for the motor to align its performance with the request imposed by the speed reference. So a Pulse-Width Modulation with 20 kHz switching frequency is used but, being absent the current sampling for control purposes, the carrier wave chosen is not triangular but a sawtooth wave obtained by using the PWM Motor Control timer in free-running mode.

The control scheme used to obtain the phase voltages is Unipolar strategy, with a single carrier wave and a two-phase-on control mode but, instead of using two complementary modulating signals for the two phases that are conducting, a single modulating signal with the amplitude of the requested duty cycle is used. The phase with the positive current in that sector will be modulated as said, the other phase will be constantly connected to down rail of the DC-link as a closing path for the current, the third phase will be fluctuating as expected.

The sensorless operation requests more care in the initial functioning, so the software integrates a start-up procedure to ensure the proper operation. As a matter of fact, the motor must be started open-loop due to the lack of BEMF information at low speed. The starting routine align the rotor to a known position. Before the motor run is run, the algorithm energizes first a pair of windings for a brief period then two pairs of windings. This procedure is very important to avoid that the position of the rotor is unstable. The last state ensures that the rotor is at a known reference point before the open loop starting algorithm begins.

At the end of alignment procedure, the system automatically starts energizing the system in an open loop stepping manner. The Back-EMF sensing technique enables a sensorless detection of the rotor position, however the drive must be first started without this feedback. The blind steps stage increases the speed as well as the amplitude of the induced voltage in order to produce sufficient BEMF voltage so the sensorless algorithm can begin operation.

The following equation is used to calculate the acceleration needed during the blind start-up procedure and can be used to obtain the time for every step.

$$\alpha = \frac{d\omega}{dt} = \frac{T_J}{J} = \frac{K_t \cdot I_{ph}}{J} \left[\frac{rad}{s^2} \right]$$

Where:

- α required acceleration,
- T_J torque required for the application,
- J sum of the load and rotor inertia,
- K_t torque constant of the motor,
- I_{ph} motor current.

3. Experimental implementation

In this section will be described all the work that has been done on the board in order to obtain the proper operative status and the requested performances, meanwhile some of the experimental results of the functioning of the drive will be presented, mainly oscilloscope screenshots and some excel graphical reconstruction of the data taken from the board, together with pictures of the workstation where everything was tested.

3.1. Preliminary work

Before implementing the actual motor control on the board, considering the operating status formerly described, some configuration modifications needed to be done in order to realize all the part of the proposed closed loop command algorithm.

The first parameter to be configured has been the PWM carrier wave. Its previous wave form was a sawtooth wave obtained by using the timer counter in free running mode. The change made consists in using the PWM time base in a continuous up/down counting mode in order to obtain a triangular carrier wave, the reason of this choice concerns the current control logic and the ADC sampling of the electrical parameters of the drive.

For linear torque control, it is important to sample the average phase current as feedback to the current regulator. One possible way to get this information is from the DC link current using only a shunt resistor because of its low cost and simplicity. However, the DC link current is not continuous and is present only during PWM on time. Another option is to sample the load current, as a matter of fact, the switching frequency, PWM on time and load inductance are such to ensure that the load current is continuous. A close look at the load current waveform in Figure 12 (left) reveals that its average value is equal to its instantaneous value during the middle of PWM on time or off time. Since the load current flows through the DC link during PWM on time, sampling the DC link current during the middle of PWM on time gives the average load current.

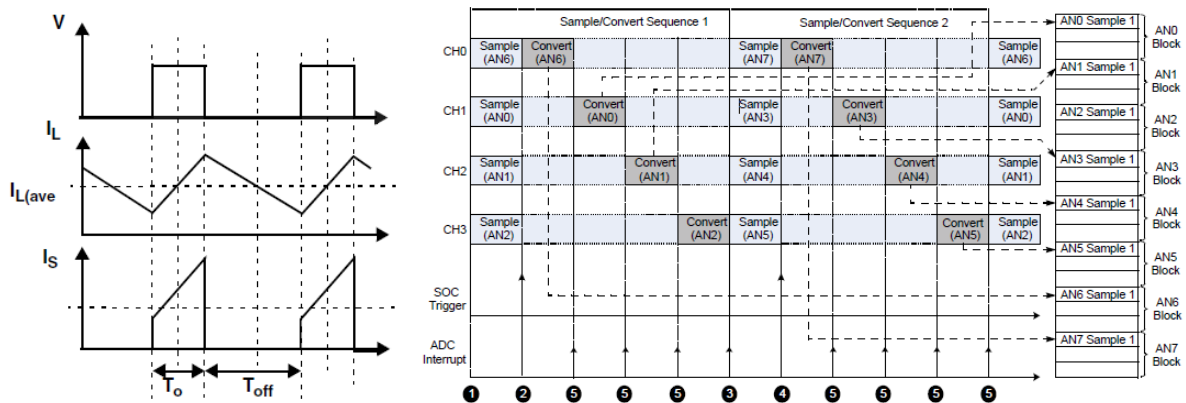


Figure 12: Current sampling synchronization (left), events sequence of ADC sample and convert routine (right)

An update strategy needed to be chosen during this preliminary phase so, considering the ADC sampling and converting speed, the switching frequency and the considerations on the instability caused by an oversampling approach, the chosen one was the ‘one sample one refresh’ technique. This consists in sampling once every switching period and updating the duty cycle calculated after the processing of the acquired data at the end of the same period, again, once every period.

The switching frequency chosen for the application is 20 kHz, the same it was previously used, this ensures a good update frequency and enough time (50 μ s) to complete the operations the controller needs to fulfil. The ADC module has been set to simultaneously sample 4 channels with a 10-bit configuration that enables 4 S&H and up to 1.1 Msp. The parameters sampled are the three phase currents and the DC-link voltage; for the current loop was enough to sample only two of the three phases but, given the

already present current sensor and the availability of one ADC channel currently unused for other purposes, it was chosen to sample all the three values and use them for the control routine. The VDC value was chosen to allow a dynamic adaptation of the duty cycle calculation: even if supplied by a bench power supply, the voltage is subject to fluctuation that can influence the normalization during the computation of the duty cycle value. According to the ‘one sample one refresh’, the sampling frequency has been set to 20 kHz, the same as the PWM. So, every time the timer ends one period, counting from zero to the value inside the Time Base Period Register and counting down again to zero, when the PWM interrupt starts, a sampling and an update event occurs, thus beginning the routine.

In Figure 13 can be seen a part of the sequence developed: the purple rising edge represents the beginning of the Interrupt Service Routine of the PWM control, from there a series of events occurs in quick succession:

1. The first operation at the start of the ISR is the data collection. As said, the interrupt corresponds with the lower peak of the triangular carrier wave. It also corresponds with the middle of the PWM on time, as can be seen by the two phase voltages in blue and green, this instant is chosen to coincide with the mean value of the phase current (yellow wave). Therefore, the operations connected to this edge are the end of the sampling and the start of the conversion.
2. The next phenomenon is well represented in Figure 12 (right) where can be seen how the four channels involved capture the value when the trigger sets in, then from a simultaneous sampling the ADC starts the series conversion. Each channel is converted one after the other producing an interrupt at the end of every conversion, the last interrupt overlaps with the DMA interrupt, this indicates that the memory has been filled with the new values and the conversion is ended. The evidence of the actual process realized on the board is reported in Figure 13, the four spikes of the digital channel are ADC interrupts and the purple falling edge represents the starting of the DMA interrupt and the conclusion of the conversion stage.
3. The just ended conversion automatically triggers the sampling that will be enabled until the next PWM interrupts requests to acquire the values and convert them to use them for the routine.
4. Once the conversion has ended the control routine can start. The current values are used as feedback in current loop, but this stage duration can change according to the control chosen. Considering a current loop control the routine will include the PI regulator which will have a voltage reference output, the duty cycle calculation according to the VDC voltage and finally the adaptation of the calculated value to the microprocessor registers.
5. The end of the routine and the storage of the duty cycle just processed will happen sometime before the end of the switching period.
6. The next purple rising edge instead indicates when the new value is passed by the DSP pins to the driver and to the gate circuit of the FETs, updating the voltage mean value desired and starting the routine all over again.

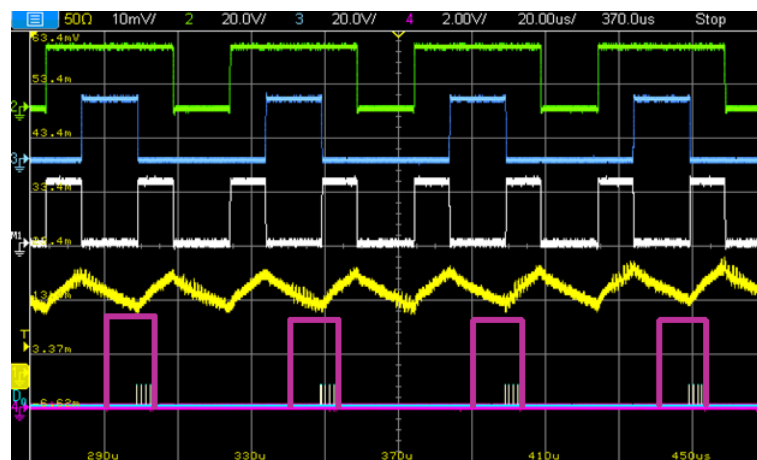


Figure 13: Sample and convert routine on the real system. Green: phase a voltage, Blue: phase b voltage, White: phase-to-phase voltage, Yellow: phase a current, Purple: LED signal used for diagnostic, PWM interrupt and DMA Interrupt, Digital channel: ADC interrupts

One of the limits of this approach is the delay that is introduced by sampling the current. As can be seen in Figure 14, the k -th current sample is used after one whole commutation period T_p to generate the k -th update. This is something that can not be avoided, as described the control routine needs time to complete the calculations. Some feedforward control techniques use the drive known features and model to anticipate the dynamic evolution of the parameters and try to eliminate, at least partially, the intrinsic delay existent in the motor control strategies. Some of these techniques will be later discussed.

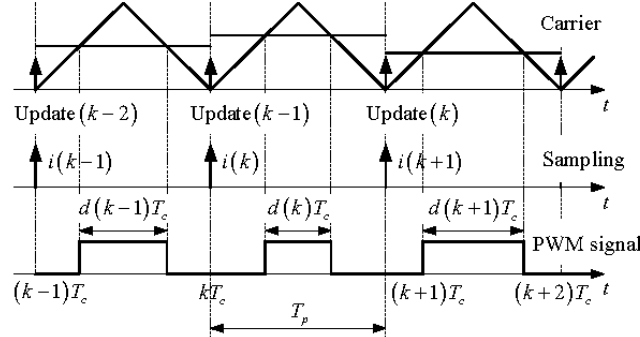


Figure 14: Sampling and updating sequence. Note: the PWM signal is the opposite of how actually calculated on the board

Another aspect to be considered during this initial set up is the sector definition. The importance of this part has been already discussed and it requires attention because, even in an open loop control, the structure of the Brushless DC drive requests an accurate position feedback and definition of the involved quantities. Referring again to Figure 5, the sector definition consists in collecting the position reference by the hall sensors and use this to determine the feedback current and the conducting phases for that sector.

About the feedback current, in a two-phase-on operation there are two possibly useful currents that, paying attention to their sign, can be used indifferently for the control loop and this was the strategy previously used but, in order to implement a bidirectional logic, a different approach is needed. In every sector, there will always be one current not commutating, one current changing its status from zero to the requested value and the last one changing its status from the requested value to zero. Depending on the rotating direction the currents that undertake these roles are different but, the one changing from the requested value to zero is the same regardless of the direction, instead the current not commutating varies and it is the one chosen as a feedback in control loop. Considering the dynamic evolution during commutation, comparing the absolute value of the two currents left, the non-commutating one will be bigger than the one changing from zero to the requested value, as imaginable. Carefully mapping the role of each current for every sector and for both the rotating directions, considering any possible misalignment between stator phases and hall sensors, a bidirectional logic can be implemented, this will allow to operate with both positive and negative references, even using simple on/off cheap sensors like the hall effect ones.

The definition of the conducting phases follows the same principle, correctly mapping the sectors and the phases involved in the torque generation, for each one of them two phases will be chosen while the third will be off. This process is implemented by using the variables pwm_a , pwm_b , pwm_c , they can be equal to +1, 0, -1 for obvious reasons. Instead the voltage imposed on the phases' terminals is calculated by the division v_{ref}/V_{DC} . The product $pwm_* \cdot v_{ref}/V_{DC}$ would be enough to calculate the duty cycle of each phase if the carrier wave variation interval was between -1 and 1 and the imposed voltage on the terminals changed between $+V_{DC}$ and $-V_{DC}$. Considering instead that the carrier wave varies between 0 and 1 and the voltage applicable is between Ground and V_{DC} , the equation to calculate the duty cycle of each phase is the following:

$$duty_a = pwm_a \cdot \frac{1}{2} \cdot \frac{v_{ref}}{V_{DC}} + \frac{1}{2}$$

The problem in this case regards the fluctuating phase, a 50% duty cycle is imposed as a result of this equation but, operating on the processor's registers, it is possible to eliminate any command passed to the driver and the gate circuit, leaving the phase off.

The outcome of using two complementary modulating signals and one carrier wave has been already discussed and it is shown in Figure 3 and Figure 13 (right). The Unipolar technique creates phase-to-phase voltage and a current ripple at 40 kHz despite the refresh frequency is set at 20 kHz, for this reason the harmonic spectrum of the current has components at higher frequencies which means their magnitude decreases more rapidly. The result is a lower current ripple magnitude, a lower torque ripple and all the consequences they all mean (lower harmonic content, joule losses, eddy currents and iron losses, lower EMI).

3.2. Simulation

To support the experimental results obtained using the control board, a simulation was implemented using MATLAB and Simulink software. The block diagram realised was used as a preliminary test field where the control techniques were studied and optimized in a safe development environment. The scheme is composed as follows:

In Figure 15 is shown the inverter, motor and load part, this consists in pre-existent SimScape modules that have been properly configured to respect the real system characteristics. The DC bus voltage is set to 24 V, the inverter is configured with a three-phase MOSFETs and diodes structure, the on resistance of the switches has been adapted according to the real FETs' datasheet, the motor parameters are imposed to recreate the features of BLDC motor: three phases, trapezoidal BEMF, stator resistance and inductance taken from the motor datasheet, torque mechanical input. As a matter of fact, a constant torque load is introduced, this will engage after 0.5 seconds from the start of the simulation giving the resulting effects of a load step.

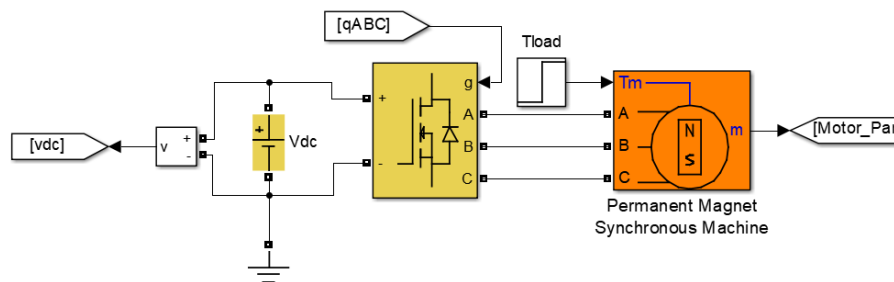


Figure 15: Simulation block diagram: supply, inverter, motor and load. Input: gate commands, output: motor parameters

The output of the motor are a set of mechanical and electrical parameters, a list of them is shown in Figure 16, the stator currents will be used to simulate the current control loop and their presence as a motor output mimics the sampling that is done in reality, the hall effect signal is a true reconstruction of the position sensors, the torque, speed and rotor angle instead are obtained by the motor model and equations, so they need to be carefully used in the simulation, they are continuous quantities which no existent sensor can re-enact.

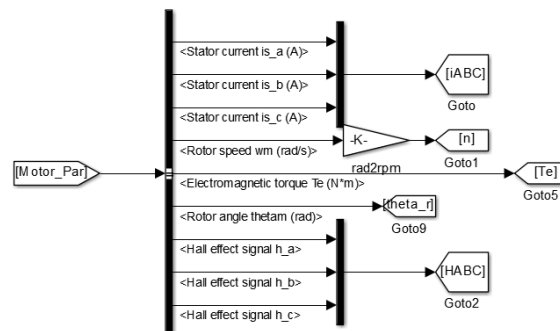


Figure 16: Motor parameters used for the drive control

These are just some of the output parameters coming from the motor block, some of them are used for diagnostic and visualizing the dynamic evolution of the phenomenon during the simulation, others are useful for the drive control and command logic implementation.

In Figure 17 is represented the block diagram of the control part. The inverter module just described, besides the voltage bus input and the three-phase connection to the motor, needs as input another signal that ensures the correct functioning of the system. The letter g symbolizes the gate command that the inverter needs to generate the commutations and then the three-phase voltages, this command is created by the control system, according to a series of input, output and internal coded schemes.

The inputs passed to the scheme come from different sources. There are the references, three values for the three kind of control developed, open loop, current loop and speed loop, the control routine is selectable from the mask menu, there are the hall sensors' signals, real and reconstructed values obtained observing the zero crossing events of the BEMF of the stator windings, these would allow to simulate a sensorless control. There are also two fictitious buttons that simulate the transition inside the states 'wake-up' and 'ready' of the control routine. Other inputs are the PWM interrupt signal, the V_{DC} voltage used to generate the duty cycle, the stator currents, the speed and rotor angle used as a feedback for the control routine as previously said.

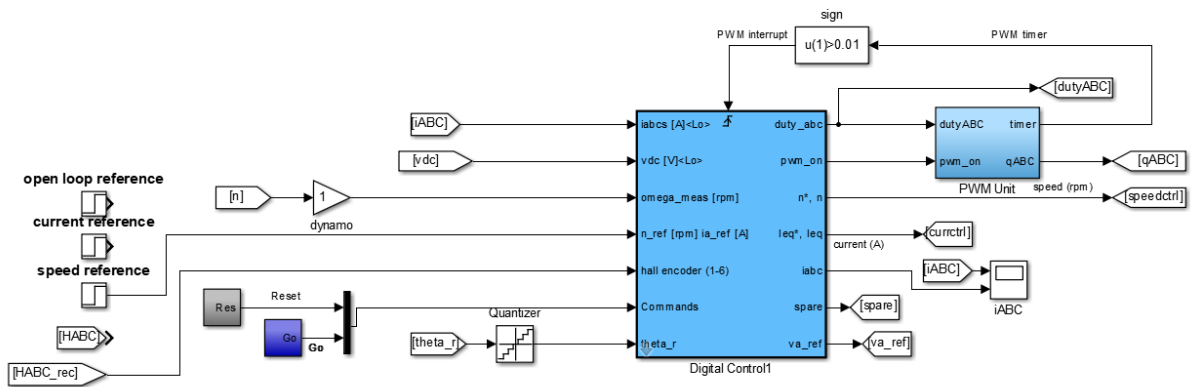


Figure 17: Digital control block diagram, gate command generator block, inputs and outputs needed for the control

The speed and rotor position values were firstly introduced to be used respectively for a speed and a position loop, later the rotor position has taken the role of both. Introducing a quantizer module is possible to generate a position signal with the same discretization of the hall effect sensors, this signal can then be used as a more accurate way of calculating the speed starting from a rough, simple signal, as for the real system.

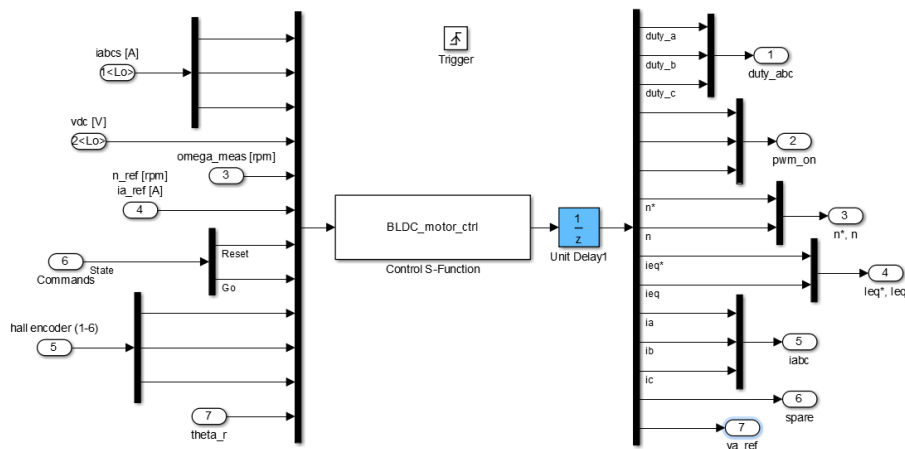


Figure 18: Under the Digital Control mask, inputs and outputs management and MATLAB S-Function block

The outputs are mainly diagnostic, useful to graphically visualize the evolution of the system, except for the values `duty_abc` and `pwm_on`, these are the results of the sector definition and the control routine

PI regulation. They are passed to the block PWM Unit which will process them and use to produce the gate command to command the inverter switches

Finally, in Figure 18 there is the scheme under the mask of the Digital control block. It does not present many more elements, the inputs and the outputs are the same already discussed, only with mux and demux elements that give an idea of the total number of the parameters, but the important part is the block S-Function. This block creates an interface between Simulink and MATLAB environment: in MATLAB is possible to implement the control algorithm as it would have been done on a real microcontroller, acquiring the inputs, calculating the duty cycles and generating the outputs for the analogic system, while in Simulink it is possible to implement the block diagram that handles these signals and generates the simulated response of the physical world. The S-function system is sometimes used also to finer simulate the behaviour of the power conversion stage and even the motor, it all depends on where the analysis focus was placed in the study of the phenomenon.

The results of the simulation will be later illustrated, side to side to the real system experimental outcomes.

3.3. Brake bench implementation

In this section will be explored different solutions for braking structures and their features, including advantages and drawbacks, in the end will be described the solution chosen and implemented for the application.

When a process consists of several drives where one motor may need braking capability when others are operating in motoring mode, the common DC bus solution is a very effective way to reuse the mechanical energy. A common DC bus solution drive system generally consists of a separate supply rectifier converting AC to DC, when present, and inverters feeding AC motors connected to the common DC bus. One of the possible problems of this configuration is the DC bus voltage rising, it depends from many factors like how much braking power is used and how the bus capacitors were sized. In general, it is necessary to consider ways to prevent an excessive rise, due to its possible catastrophic effects.

Two possibilities are available: the first consists in the inverter itself preventing the power flow from process to the drive. This is done by limiting the braking torque to keep a constant DC bus voltage level. This operation is called overvoltage control and it is a standard feature of most modern drives. However, this means that the braking profile of the machinery is not done according to the speed ramp specified by the user. The other possibility to limit DC bus voltage is to lead the braking energy to a resistor through a brake chopper. The brake chopper is an electrical switch that connects DC bus voltage to a resistor where the braking energy is converted to heat. The brake choppers are automatically activated when the actual DC bus voltage exceeds a specified level depending on the nominal voltage of the inverter.

The chopper and resistor solution is appealing for different reasons: first of all its cost, it is a well-known technology made with cheap and simple components with a great availability, then, being a passive braking system, it does not depend from the reliability of the software control effectiveness or even by the presence of voltage supply, which can be useful in many application where a safe, always present braking intervention is requested. Many drawbacks are also present, like the higher system losses due to the power wasted in the resistors, the additional space requested by the structure linked also to the sometimes needed extra cooling and heat recovery system, the safety of the structure due to hot resistors and variable DC-link voltage and some other. Nevertheless, the solution is used when the braking cycle is needed occasionally or the amount of braking energy with respect to motoring energy is extremely small.

The solution adopted for the thesis application uses the concepts just described with some modifications. Two equally powerful motors (65 W BLDC) are coupled together allowing them to rotate at the same speed. One of them is connected to the board and it is controlled with the different routines that will be discussed later, the other one is dragged by the first one that engages the motor role. The braking effect is obtained by connecting the braking motor terminals to resistive load, to be specific the three-phase

terminals producing three-phase trapezoidal BEMFs are linked to an AC rectifier stage, this is an uncontrolled three-phase bridge composed by six diodes. The high and low rail of the bridge are connected to a resistive load like shown in Figure 19.

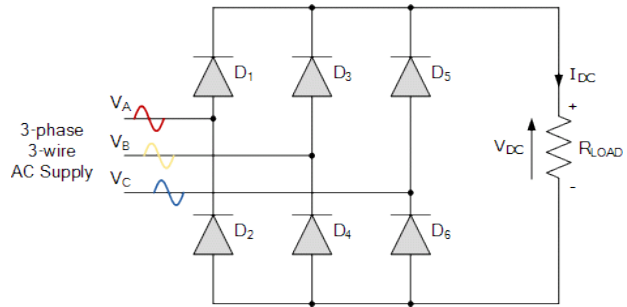
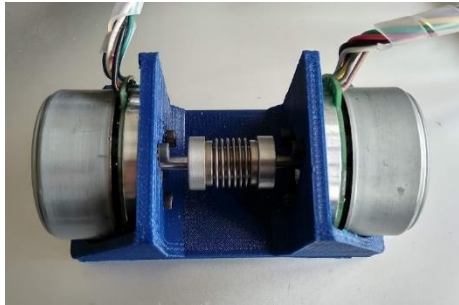


Figure 19: Brake bench 3D printed prototype (left), electrical load connected to the dragged motor (right)

The main difference is that instead of connecting the DC interface of the rectifier to the DC bus and then using a brake chopper and resistor, the solution chosen uses resistors directly on the rectifying stage. Moreover, the resistive part is composed by three 50 W resistors in a parallel configuration that can be connected or disconnected creating a three-level discrete load resistance. If more variability is requested an interface to connect in parallel an electronic DC load is available, this can ensure more load levels and a finer regulation of the braking performance offered by the brake bench.

3.4. Fixed-point implementation

Digital signal processing can be separated into two categories, fixed point and floating point. These designations refer to the format used to store and manipulate numeric representations of data. Fixed-point DSPs are designed to represent and manipulate integers, positive and negative whole numbers, via a minimum of 16 bits, yielding up to 65,536 possible bit patterns (2^{16}). Floating-point DSPs represent and manipulate rational numbers via a minimum of 32 bits in a manner similar to scientific notation, where a number is represented with a mantissa and an exponent, yielding up to 4,294,967,296 possible bit patterns (2^{32}).

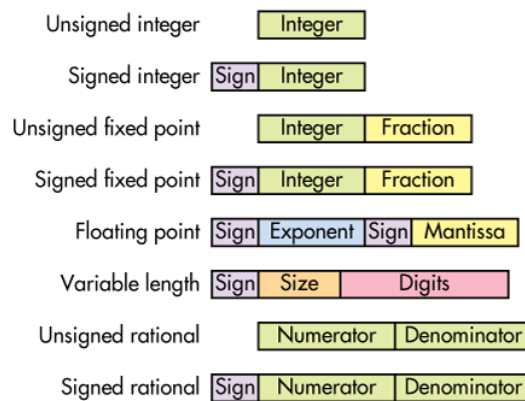


Figure 20: Number representation in processor architecture

The term ‘fixed point’ refers to the corresponding manner in which numbers are represented, with a fixed number of digits after, and sometimes before, the decimal point. With floating-point representation, the placement of the decimal point can ‘float’ relative to the significant digits of the number. The exponentiation inherent in floating-point computation assures a much larger dynamic range, which is especially important when processing extremely large data sets or data sets where the range may be unpredictable. As such, floating-point processors are ideally suited for computationally intensive applications.

It is also important to consider fixed and floating-point formats in the context of precision and the size of the gaps between numbers. Every time a DSP generates a new number via a mathematical calculation, that number must be rounded to the nearest value that can be stored via the format in use. Rounding and/or truncating numbers during signal processing naturally yields quantization error or ‘noise’, the deviation between actual analog values and quantized digital values. Since the gaps between adjacent numbers can be much larger with fixed-point processing when compared to floating-point processing, round-off error can be much more pronounced.

Because fixed point operations can produce results that have more digits than the operands, information loss is possible. For instance, the result of fixed-point multiplication could potentially have as many digits as the sum of the number of digits in the two operands. In order to fit the result into the same number of digits as the operands, the answer must be rounded or truncated.

The work made on the DSP board was done following a fixed-point logic. In order to minimize the effects and toughness of the algorithm implementation, all of the used numerical variables were declared either as unsigned or signed integer. Every time a fractional number was involved it was scaled and then used according to the operation just done. Due to the presence of numerous mathematical operations, particular attention was paid in the occurrence of an overflow event. As previously said the use of multiplications implies the need of long integers with higher bits number, this is necessary to avoid loss of information and a lower precision.

Another aspect to be considered is the computational burden created by the division and more complex calculations. The importance for the control routine to finish in time before the intervention of another ISR is crucial to ensure the real time action of the control algorithm. With this in mind, a lot of work was made towards the optimization of the computational process of the PI regulators of the closed loops control, most of the divisions, except when essential, were adapted to shifting operations, the same for some multiplications, when possible and convenient, then complex operations with lots of sums, multiplications and divisions were simplified as much as possible in order to minimize the clock shots needed to complete the computation.

All of these aspects, even if neglected during the code implementation of the simulation, have a key role in the correct functioning of a real time physical structure and the knowledge of the theory of the phenomenon involved is essential when working on these structures.

3.5. Open Loop

The open loop control strategy, also called V/Hz control, consists of imposing a voltage reference to the motor terminals and let the rotor turn freely without any motor feedback. Usually this kind of control is used as a diagnostic mean to make sure all the preliminary work is correctly done and is properly operating. As a matter of fact, the workstation during this phase needs to be staged with current probes, speed sensors and software testing and debugging tools to analyse the code processing and results.

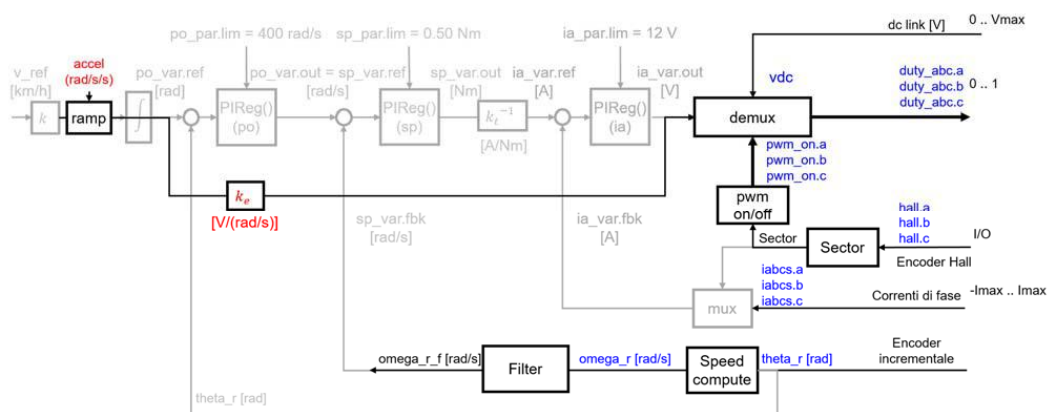


Figure 21: Open loop control, focus on the digital control part

For the case of the BLDC drive some particular precautions need to be addressed when using an open loop technique: the easy part, similar to the way a DC motor is controlled in open loop, is the definition of the reference voltage starting from a reference speed, the conversion factor k_e allows to jump all the closed loop regulations and calculate the duty cycle needed, while the division into sectors of the motor circumference implies the voltage command can not be simply applied to the stator terminals. The sector sequence needs to be respected and the voltage command needs to be applied two phases at a time like every other control scheme, this can be done with a feedback or feedforward mechanism: if the algorithm waits the hall effect sensors signal to understand in which sector the rotor is and then chose the phases that need to be energized, it is considered a feedback control, even if in its simplest form, if the phases are chosen a-priori without waiting for the sensor information, it is a feedforward control.

The feedforward control applies blind voltage steps in order to create torque and rotate the motor at a constant speed, this is a starting point for the diagnosis of the correct functioning of the various software parts. In this condition the first parameter to be analysed is the correct definition of the sectors, if the motor rotates and the voltage and current signals have the right waveforms the first accurate characterization has been made and the next step is the verification that the hall sensors signals agree with the sector definition just supposed. Next there is the current measure: using current probes directly applied on the motor terminals is possible to confront the actual current value with the signal produced by the sensors on the PCB and then retrace the signal path considering filtering, conditioning and adaptation to the unit of measure used inside the software.

In this thesis the open loop control was obtained by using the routine of a speed loop control and then bypassing all the internal loops calculation to give the final voltage command as feedforward signal. This allowed to let the algorithm run without influencing the command law of the motor and made possible to implement step by step the wanted logic in a continuous trial and error that verified the assumptions made and corrected the mistakes made in the preliminary part.

So after the current measure verifications, the debugging tools are useful to validate the current loop steps functioning, from the error computation, the PI regulator with its gains and to the output generation. The same process is done for the speed loop: the part of the algorithm responsible of the speed estimation is complex and requested many trials before the performance offered by the speed loop was acceptable, so it is easy to understand the importance of this phase where the speed value stored in the software variables was compared with the forecast made and with the actual value measured on the motor by an optical tachometer. Various attempts were made, they will be discussed in the specific section, and after the usual verification of error computation, PI gains tuning and output generation it was possible to proceed with the actual motor and parameters control.

The next images represent all the phenomenon until now described, they are the results of all the studies and the work done and need a higher attention, particularly for some details.

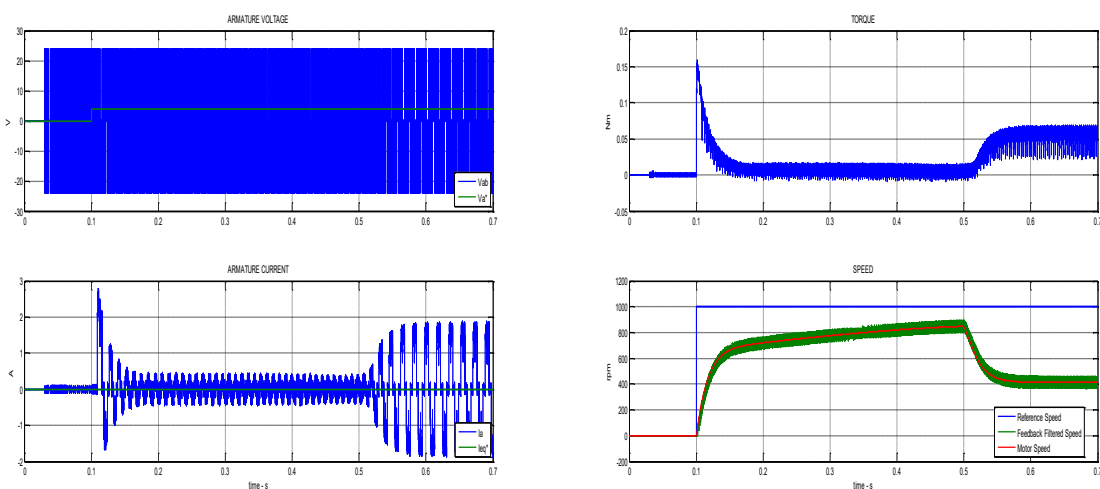


Figure 22: Open loop simulation. UP: Green, reference voltage; Blue, phase voltage, DOWN: Green, reference current; Blue, phase current (left), UP: torque; DOWN: Blue, reference speed; Red, actual speed; Green, filtered speed (right)

Figure 22 shows the prints of the simulation developed: the left image has some electrical parameters such as phase-to phase voltage, reference voltage, phase current and reference current, while the right image has some mechanical parameters like torque, reference speed, actual motor speed and filtered speed. The simulation has the following features:

- 1000 rpm reference speed;
- 75 Hz cut-off frequency for the speed filter;
- 0.05 Nm torque load applied at 0.5 s.

A step command has been given to the system in order to observe the drive response and a 1000 rpm reference was chosen to reduce the starting currents and torque so as to avoid the protection intervention. Things to notice are the quick start phase with the speed rising abruptly and the high phase current and mechanical torque, then a saturation phase where the actual speed can not respect the reference imposed due to the higher inertia imposed by the dragged motor and finally the load insertion that asks for more torque and obviously current and decelerates the rotating speed due to the absence of a feedback control.

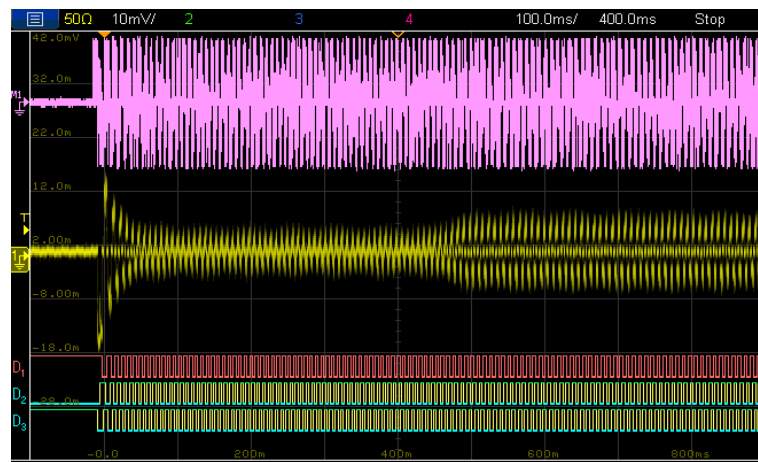


Figure 23: Oscilloscope screenshot of real system functioning. Pink: phase-to-phase voltage, Yellow: phase current with probe 2 A/div, Digital channels: hall effect sensors

In Figure 23 is represented the real unrolling of the process, it has been chosen to recreate the same conditions implemented in the simulation so to verify the accuracy of the model created and the goodness of the algorithm developed on the board. Using two analog channels for phase voltages it was possible to obtain the phase-to-phase voltage in pink as the difference between them, then another analog channel was used to connect the current probe set to 2 A/division and finally three digital channels were used to scan the hall effect position sensors. Unlikely it was not possible to acquire a speed measure signal, as a matter of fact the rotor did not have an encoder sensor mounted the speed estimation used for the speed control was obtained by software using the hall sensors. An external tachometer was used for the verifications during the work, but its data were not available to be visualized on the oscilloscope.

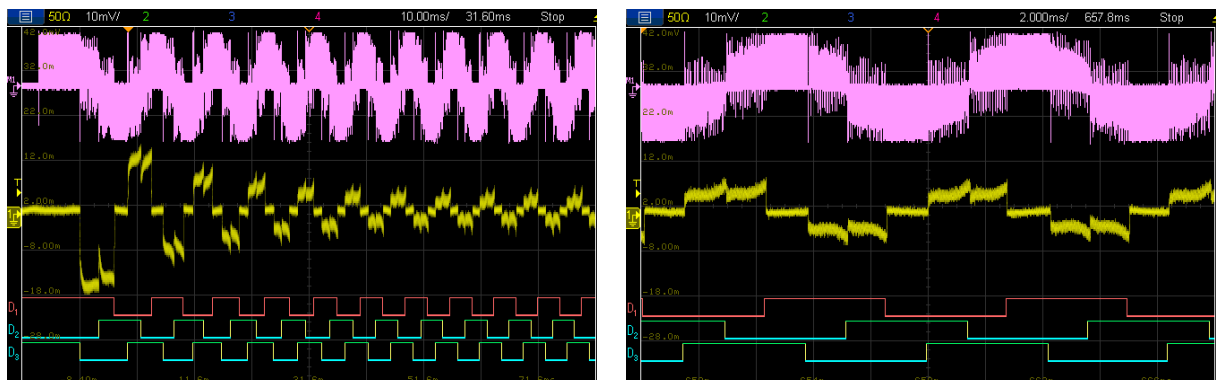


Figure 24: Oscilloscope screenshot of real system functioning. Pink: phase-to-phase voltage, Yellow: phase current with probe 2 A/div, Digital channels: hall effect sensors. Starting sequence (left), load connected regime working (right)

It is easy to recognize the three stages in the evolution of the phase current: starting, empty regime and load insertion and the correctness of the images explains how the model was precise and the control implemented was well written.

The last oscilloscope screenshot is composed by two images, the left one is an enlargement of the starting phase with the peak current and the rapid rotor acceleration, the right one is an enlargement of the regime functioning with the load connected. In these cases its clearer the evolution of the phase-to-phase voltage and the hall effect sensor, moreover the current evolution is not constrained by external loops and therefor takes this particular form, always being synched with the sector definition carried out by the hall sensors.

3.6. Current Loop

One of the modifications introduced during the algorithm implementation was about the intervention timing the routine had to have. The previous algorithm structure was based on a speed loop control with no internal current loop, this allowed a very low update frequency due to the low variability of the speed and the fact that a new signal from the hall sensors is obtained every 1/48 of a mechanical turn of the rotor. For these reasons the control was neither integrated in an Interrupt Service Routine, an external scheduler took care of timing the different routines, assigning to this one 10 milliseconds refresh period, which means 100 Hz update frequency. With the introduction of the current loop and the will of controlling electrical quantities with a much quicker variability, the performance of the algorithm needed to step up, to be specific the update frequency, as previously explained, has been upgraded and synched to the switching frequency of the inverter, so up to 20 kHz. This value needs to be carefully chosen because a too low update frequency does not ensure the proper domain of the current and can mean malfunctions and overcurrent protections interventions, while a too quick algorithm can lead to oversampling and instability which can be equally dangerous.

The current control, also called I-Hz control, is an adaptation of a torque control, the one called machine control, this has a tight link with motor nature, its physical structure and the mechanical and electrical phenomenon involved. The transition from torque to current occurs through the torque constant k_T , this is a feature of DC and BLDC motors only that allows a great simplification of the management of the drive quantities. As already said, the torque measure is obtained with mechanical sensors that are expensive, cumbersome and difficult to manage and analyse, current measure is instead cheap, space-saving and available in different solutions.

Part Number	Packing*	T_A (°C)	Optimized Range, I_p (A)	Sensitivity, Sens (Typ) (mV/A)
ACS712ELCTR-05B-T	Tape and reel, 3000 pieces/reel	-40 to 85	±5	185
ACS712ELCTR-20A-T	Tape and reel, 3000 pieces/reel	-40 to 85	±20	100
ACS712ELCTR-30A-T	Tape and reel, 3000 pieces/reel	-40 to 85	±30	66

Figure 25: Current sensor data-sheet information on sensitivity

For this project it was decided to use hall effect current sensors mounted on the three inverter's legs. In Figure 9 can be seen the sensor of one of the legs and a shunt resistor connected to the ground, this is used for the measure of the DC bus current, which can be useful in several circumstances, as already said, but it is currently used only for diagnostic reasons and possibly to study which solution can be better in order of accuracy, resolution, affordability, reliability and ease of use.

The first solution was a 30 A full scale sensor which can be useful for higher power applications, but its use on a 65 W motor with nominal current of 3.26 A is wasted and not useful in terms of resolution and sensibility. Moreover, with the need of adapting the sensor signal to the 0-3.3 V voltage interval of the microprocessor, the choice of a 5 A full scale sensor was made, allowing to improve the overall performances during low and medium current operations.

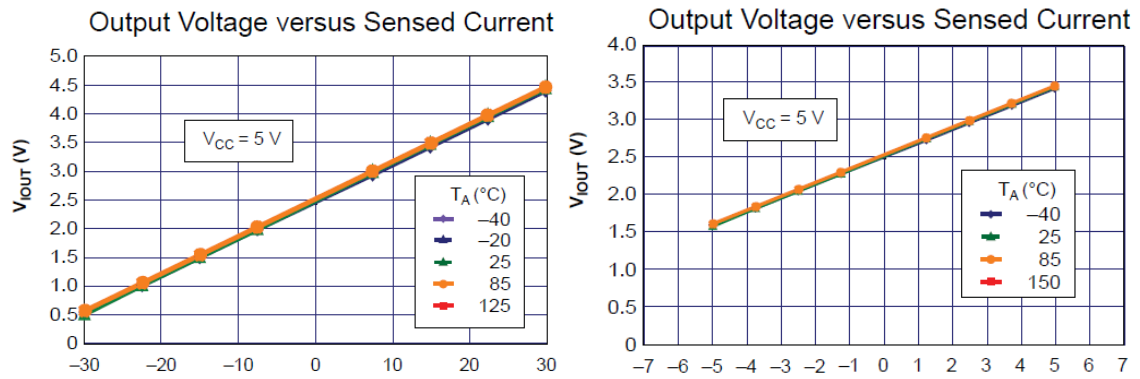


Figure 26: Current sensors full scale and voltage relationship, 30 A sensor (left), 5 A sensor (right)

Another modification made to the previous hardware setup concerns the ADC sampling, as a matter of fact the first configuration was not using a simultaneous sampling method but instead scanned the active channels converting the signals arriving at the pins one at a time. The computational burden is reduced but the low sampling frequency and the not simultaneity of the operations make the obtained values useless if not for diagnostic purposes. In Figure 27 is shown one similar configuration example, as it is reported in the datasheet description, the only channel used is the CH0 and all the input from AN0 to AN15 are scanned through the process. In Figure 12 (right) instead, as previously mentioned, is described the current configuration: all the four channels of the ADC module are used and a simultaneous sampling technique is implemented in order to obtain the parameters values every time at the same instant.

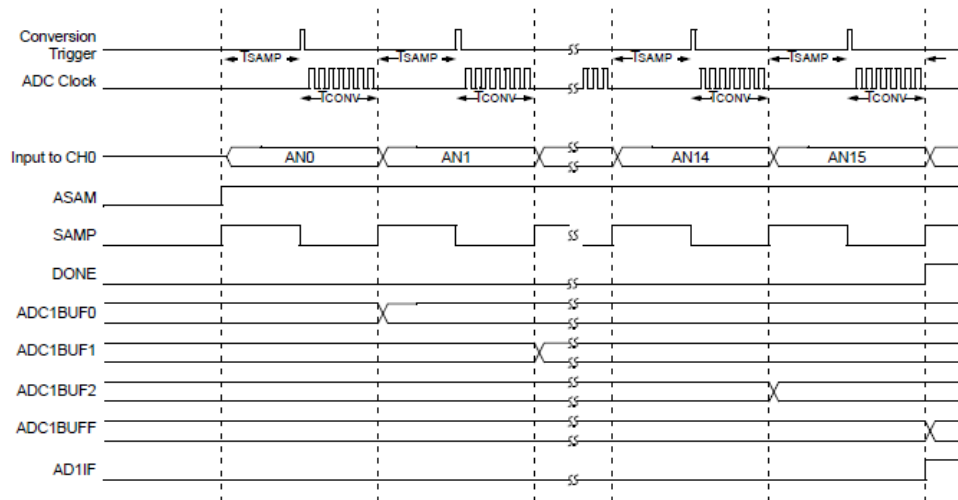


Figure 27: ADC previous functioning, the 16 pins are scanned and converted one after the other

In the next pages are reported the experimental results of the current control loop developed on the board. The configuration used is the following:

- 1 A reference current;
- 75 Hz cut-off frequency for the speed filter;
- 0.05 Nm torque load applied at 0.5 s.

Figure 28 shows the simulation outcomes, this time the reference parameter is given by a constant current which means constant torque and then acceleration. The effect should be seen in the torque diagram but the current ripple, the rotational inertia and the commutations of the switches allow fluctuation of the mechanical and electrical quantities around the requested value. Moreover, with a 1 A reference current, the torque developed in 0.0369 Nm, in this condition a higher ripple is expected due to the lower precision of the control for low load situations. Confirming the assumptions made, is possible to observe the poor performance in the current diagram were the green wave is repeatedly

outmatched by the blue one. However, the constant acceleration can be seen in the speed evolution, a straight line growing linearly according to the reference voltage.

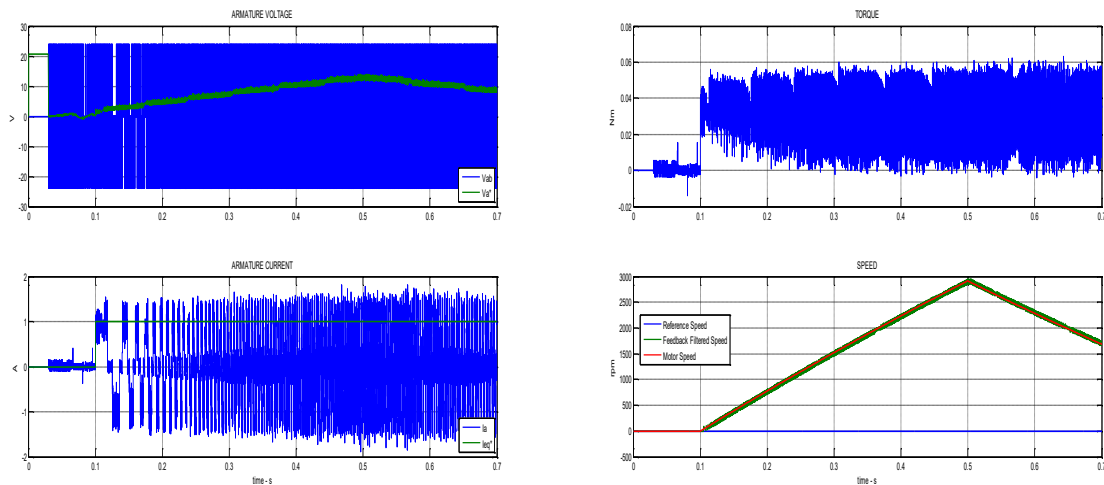


Figure 28: Current loop simulation. UP: Green, reference voltage; Blue, phase voltage, DOWN: Green, reference current; Blue, phase current (left), UP: torque; DOWN: Blue, reference speed; Red, actual speed, Green, filtered speed (right)

In Figure 29 is again represented the real system response to the proposed stimulus, the speed rise can be seen by the thickening of all the signals, but particularly the hall effect sensors, then the speed falling is equally imaginable by the rarefaction of the signals and their lower frequency subsequent to the load insertion.

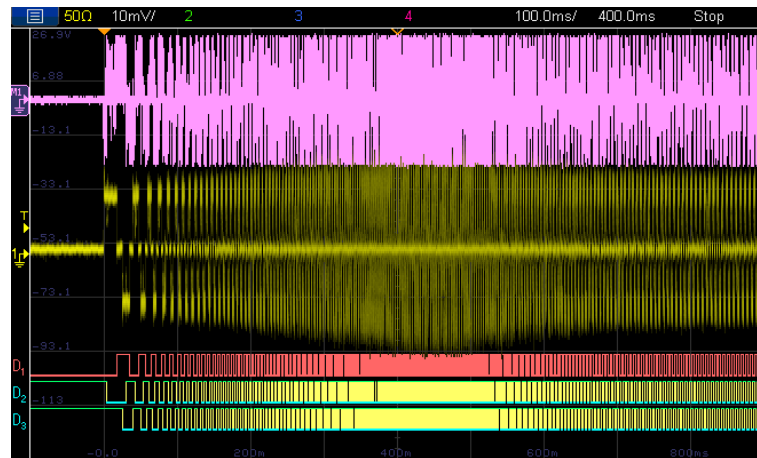


Figure 29: Oscilloscope screenshot of real system functioning. Pink: phase-to-phase voltage, Yellow: phase current with probe 1 A/div, Digital channels: hall effect sensors

In order to better analyse the events happening during the routine a magnification of Figure 29 is displayed. The respect of the imposed command, with the limits the control can observe, make understand the performance of the motor and the restrictions that need to be imposed to avoid protection intervention and improve the effectiveness of the system.

The same consideration will be now made for another case where the system setup will be:

- 2.5 A reference current;
- 75 Hz cut-off frequency for the speed filter;
- 0.1 Nm torque load applied at 0.5 s.

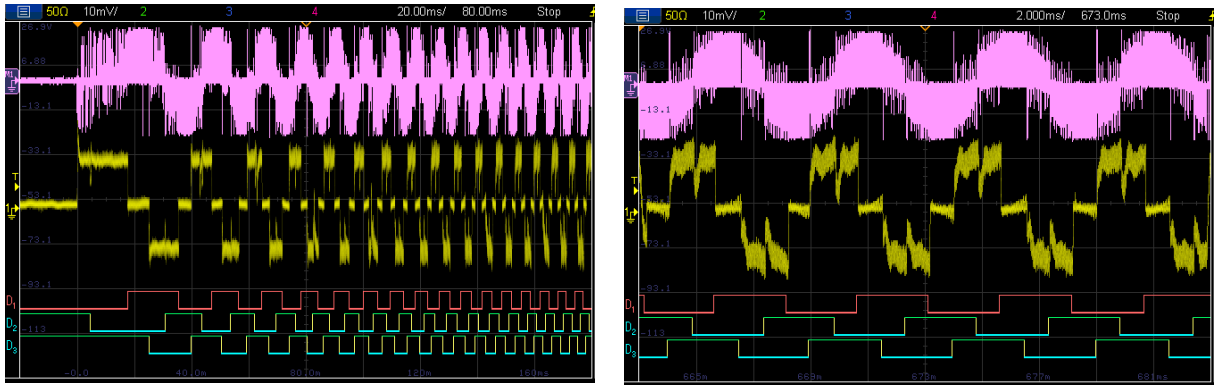


Figure 30: Oscilloscope screenshot of real system functioning. Pink: phase-to-phase voltage, Yellow: phase current with probe 2 A/div, Digital channels: hall effect sensors. Starting sequence (left), load connected regime working (right)

This new configuration is used to observe some differences: a higher current command means higher torque and a steeper speed slope. This allows the motor to reach the max possible speed in time for the end of simulation and more importantly before the load insertion.

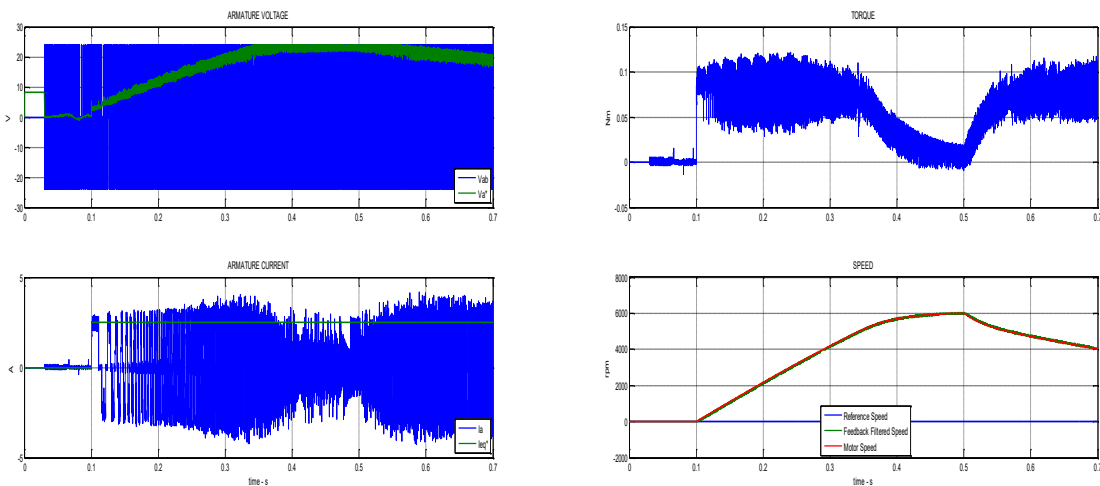


Figure 31: Current loop simulation. UP: Green, reference voltage; Blue, phase voltage, DOWN: Green, reference current; Blue, phase current (left), UP: torque; DOWN: Blue, reference speed; Red, actual speed; Green, filtered speed (right)

The phenomenon observable both from the simulation and oscilloscope screenshot is the lowering of the phase current and mechanical torque corresponding to the max speed achievement. This limit is imposed by the BEMF: when the electromotive voltage matches the DC voltage, that is the maximum voltage impossible to the stator terminals, the current can not be forced anymore and so it decreases almost cancelling the torque contribution.

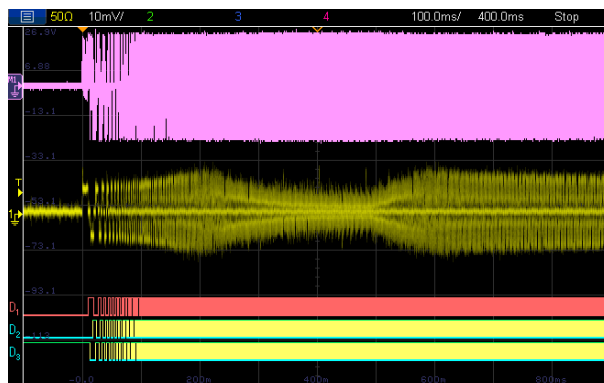


Figure 32: Oscilloscope screenshot of real system functioning. Pink: phase-to-phase voltage, Yellow: phase current with probe 5 A/div, Digital channels: hall effect sensors.

The low current stage lasts until the load insertion when the rotor slowing down process gives more voltage forcing margin, in this way the current grows back to its original reference value producing the max torque deliverable in that situation. In Figure 33 can be observed the difference between the current during starting operations and regime functioning with the load engaged: on the left the reference is respected and flat waveforms are generated, on the right instead there is a loss of control, the objective is obtained on average but the outcome is exaggeratedly fluctuating with a phase-to-phase trapezoidal voltage containing a lot of spikes and holes.

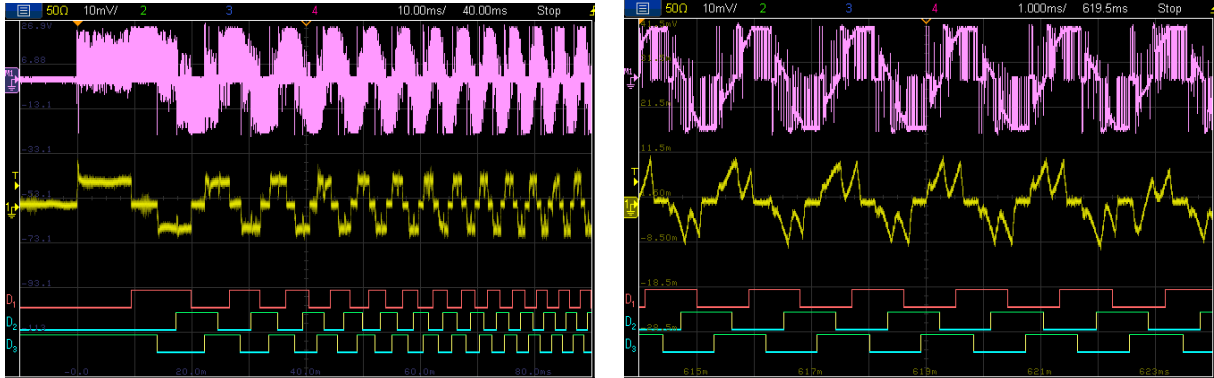


Figure 33: Oscilloscope screenshot of real system functioning. Pink: phase-to-phase voltage, Yellow: phase current with probe 5 A/div, Digital channels: hall effect sensors. Starting sequence (left), load connected regime working (right)

3.7. Speed Loop

The possibility of regulating the speed of an electrical drive is an important and useful option for a lot of applications, it requests much more attention, for the management of the speed measure and the PI gains regulating effects, and it is much more sensitive, considering the care needed for the sensor and rotor coupling and the signal conditioning.

The speed loop is a kind of control that is almost independent from the typology of motor it is applied to. This is of course an exaggeration but ignoring the internal current loop and considering its gain equal to 1, choosing correctly the bandwidths of both the loops, and analysing the inputs and outputs of the speed control it is understandable the reason of this affirmation. In a sensed drive system the feedback speed used to compare the reference is given by an external device which works on the mechanical rotation of the rotor, feature that does not resent of the electrical or magnetic model of the drive, from an external point of view. The output of the system is a voltage command that in simplest cases consist of duty cycle used to command the power conversion stage. If it is not entirely true for induction motors and in cases where a lot depends from the modulating technique chosen, the concept is perfectly applicable to the BLDC case where the duty cycle calculated in this way can be applied to the stator terminals with minimum knowledge of the device spinning. This is what was done in the previous operating status of the board, but it is something it is done for low cost, low power applications where little importance is given to the actual performances and even major malfunction may not harm significantly the whole system.

What happens between the input acquisition and output generation needs to be addressed to, as a matter of fact the regulator used, mainly a PI system tuned accordingly to the drive parameters or by trial and error methods, may affect the performances of the drive. As already known the proportional gain aims to delete the difference between reference and feedback by applying as much voltage as possible and the integral gain is used to accumulate error in order to eliminate the additive noise which, in the speed loop, is represented by the load torque. The integral regulation is often associated with a saturation module that limits the command voltage when the maximum performance is reached but its presence generates the wind-up phenomenon. It consists in a drift of the command due to a delay between the error accumulation and the saturation of the command it self so, instead of limiting the performance when the reference is reached the loop continue to apply the command increasing the speed when not necessary. The problem is solved by saturating the integral output before it starts accumulating error

instead of saturating the output of the loop leaving the integral module free to evolve and make the speed drift apart.

The motors used for the work have not a position or speed sensor mainly for size and economic reasons, adding an encoder or a tachometer on a 65 W BLDC motor with 42.8 mm diameter would mean an increase in volumes but mainly price considering the difficulty in miniaturizing a speed sensor and trying to preserve its precision characteristics. Luckily the BLDC drive can rely on another instrument to obtain information about the speed, the hall effect sensors mounted on the stator to acquire the sector occupied by the rotor can be used as a source of signals to recreate the dynamic evolution of the rotation, but their limits are obvious. The functioning principle used is the same of an encoder, the speed measure is discretized and updated every time the rotor movement meets the new notch, higher the number of notches higher will be the accuracy of the speed reconstruction and the cleanliness of the signal but, if a sensor used specifically for this purpose can have, for a medium range application, 512 notches obtaining a resolution of 0.7 degrees per notch, the hall effect sensors produce 6 edges, one rising and one falling for each sensor, on an electrical turn. This is a huge limitation which is only mitigated by the fact that the motor used for the work has 8 pole pairs, for a total of 48 pulses per mechanical turn and a resolution of 7.5 degrees.

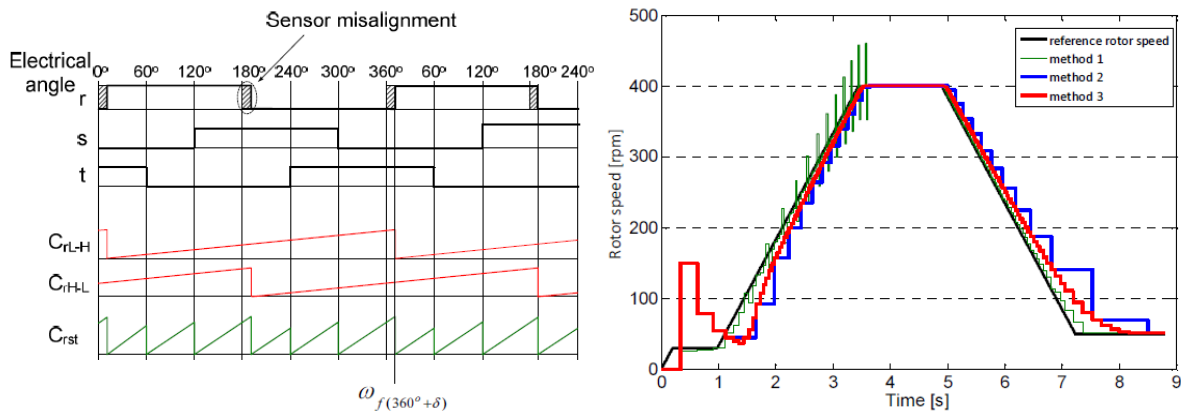


Figure 34: Misalignment. Hall effect sensors signals, position calculated starting from the signal edges (left), effect of misalignment on three speed estimation methods and corrective algorithm result

The solution used is chosen when costs need to be contained but the performance offered is not exceptional, the signal used as a feedback is noisy and generates fluctuations on the controlled speed which is just partially filtered by the motor inertia. If the oscillation is too high the effect are vibrations, noise and mechanical stress on the components. Another problem is represented by the possible misalignment of the sensors, in a small motor with 8 pole pairs and a small circumference the position of the devices is critical, one millimeter can be enough to create even more noise on the signal received and all the consequences it means. The effects of this particular feature are described in the paper “Calculation of the Brushless DC Motor Shaft Speed with Allowances for Incorrect Alignment of Sensors”. The noise increase is understandable and the cause is obvious but the paper focuses on the effects that this constructive imprecision may have on different algorithm for the speed measure: as a matter of fact the paper proposes 3 different approaches, one more accurate than the other. The misalignment affects more strongly the more accurate measure while the less accurate methods are much more insensible to the problem. Finally, the paper proposes a corrective algorithm to mitigate the problem, the effects are shown in Figure 34.

Therefore, a very popular solution consists in the implementation of a digital filter. A low-pass filter with a single time constant allows to smooth out the dynamic evolution of the measure just done. As known a strong filter with a low cut-off frequency gives a better representation of the actual speed if the average of the measured value coincides with it, so it is important to stay closer as possible to the speed frequency rejecting every superior harmonic content that creates noise. The side effects of this method are a delay in the dynamic response, higher for lower cut-off frequencies, which may not be a problem in regime operations but it actually is when is requested to the motor readiness and rapidity in responding to a given command and, from a controlling view point, the risk in pushing too hard on the cut-off

frequency is to exceed the limits of the stability of the system obtaining an instable and underdamped response. For this reason different filters have been tested during the work and thanks to the graphic results of the simulation it has been possible to choose the right bandwidth for the best performance.

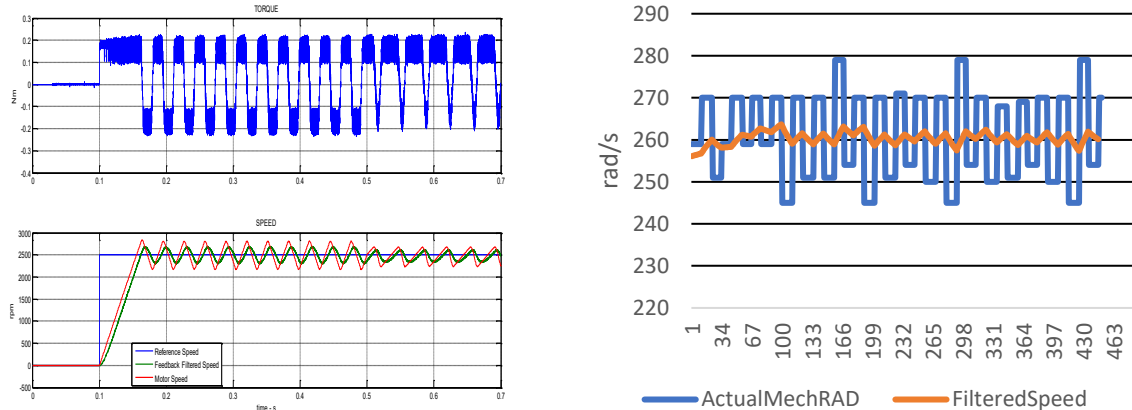


Figure 35: Speed loop simulation with 25 Hz cut-off frequency filter on the speed measure. UP: torque; DOWN: Blue, reference speed; Red, actual speed; Green, filtered speed (left). Excel reconstruction of 75 Hz cut-off frequency filter (right)

A 25 Hz cut-off filter like the one in Figure 35 (left) shows all of the features just described, the waveform reconstructed is slim and not disturbed at all, but the delay between the real speed and measured one can be clearly seen and the regime response is widely fluctuating around the reference value which is not acceptable in a speed controlled drive. On the right is instead represented a diagram with data taken from the board. The blue wave represents the speed estimation calculated by the software on the board for a 2500 rpm (261 rad/s) operating status, the data acquired are transferred on an Excel sheet where a 75 Hz cut-off frequency filter is applied. Here it is not possible to observe the evolution of the system with different filtering levels, but it is a preliminary way to analyse the effects of different methods before the practical implementation.

Given the poor outcome of using a filter with a cut-off frequency too low, a 75 Hz filter was used and the result is shown in the following images. The conditions in which the data were collected are:

- 2500 rpm reference speed;
- 75 Hz cut-off frequency for the speed filter;
- 0.1 Nm torque applied at 0.5 s;
- 5 A max current.

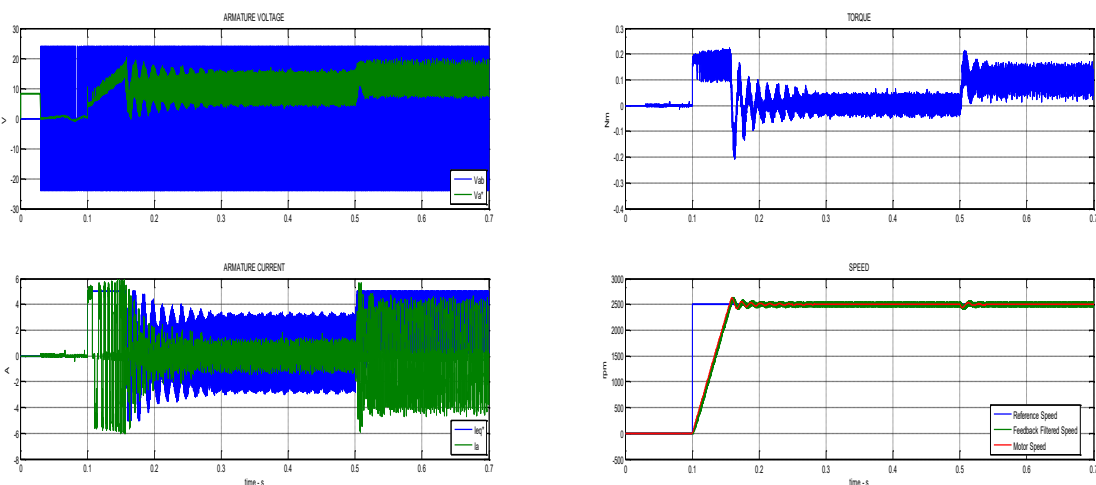


Figure 36: Speed loop simulation. UP: Green, reference voltage; Blue, phase voltage, DOWN: Green, phase current; Blue, reference current (left), UP: torque; DOWN: Blue, reference speed; Red, actual speed; Green, filtered speed (right)

The simulation shows the system behaviour to the usual stimuli: a command step, the achieving of the regime with no load, the load insertion and the response to it. The control loop allows the quickest dynamic evolution during the first instants, then a little overshooting and some fluctuation before the regime, the torque and current diagrams visualize how these parameters behave when trying to eliminate the error in the beginning and then inverting the sign of the value when compensating the oscillations of the speed around the reference command. The current in this case is generally noisier considering it is controlled by the external loop and its variation is due to the will of the all system to respect the objective and dampen any disturb influencing the control. The goodness of the algorithm developed is then expressed by the ability of being almost completely insensible to the load insertion, a minimum oscillation can be seen and an immediate increase of both torque and phase current, but the drive is ready and the reference is respected without hesitations as it was expected.

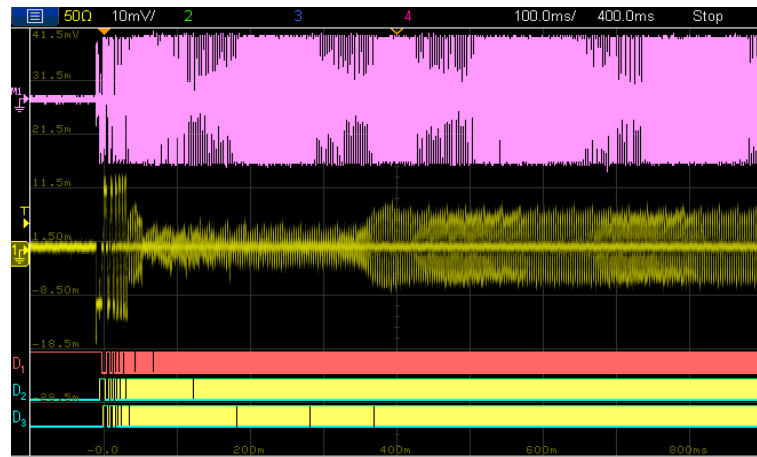


Figure 37: Oscilloscope screenshot of real system functioning. Pink: phase-to-phase voltage, Yellow: phase current with probe 2 A/div, Digital channels: hall effect sensors.

The real system evolution is the expression of all the work until now done, just as in the simulation the stages are the same: main acceleration at the beginning with the limitation of the torque produced by restricting the max current value to 5 A, overshoot compensation with torque oscillating between positive and negative values to eliminate the speed fluctuations, empty regime with very low current and finally the load insertion with the increase of the magnitude of the current virtually with no major variation on the speed value.

The absence of a visualization of the actual speed of the motor is a flaw of the diagnostic system, even if the respect of the reference has been verified with external instrumentations. However, other parameters can be analysed and they are shown in Figure 38 where enlargement of the starting operations and of the load regime functioning are presented. A better visualization of the phase-to-phase voltage and the thickening of the hall effect sensors signals makes understand how the evolution of the drive agrees with the outcome of the simulation and the algorithm works between the boundaries imposed and natural limitations of the system.

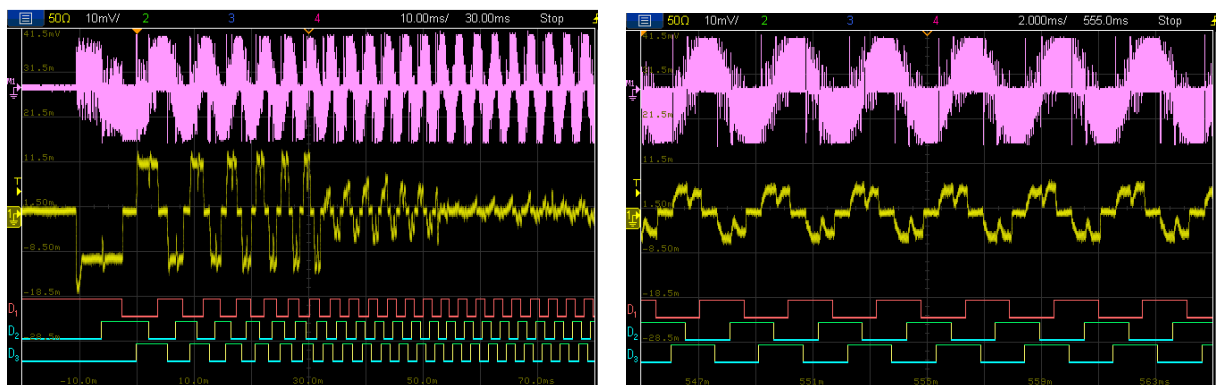


Figure 38: Oscilloscope screenshot of real system functioning. Pink: phase-to-phase voltage, Yellow: phase current with probe 2 A/div, Digital channels: hall effect sensors. Starting sequence (left), load connected regime working (right)

3.8. Sensorless control

The term sensorless refers to those applications that do not require speed and position sensors to determine the rotational performance of the motor. This kind of control relies on other mechanisms that are different from one motor to the other given that they exploit particular constructive features, physical characteristics and the electric and magnet model of the whole drive system.

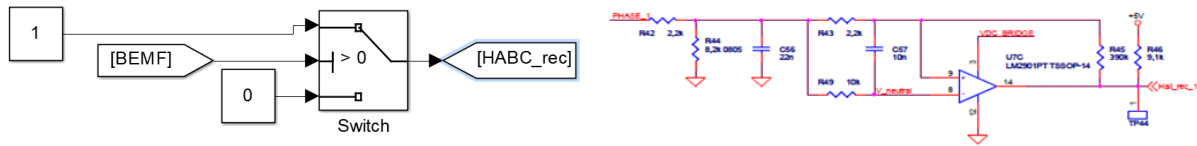


Figure 39: Zero-crossing detection circuit for back-EMF in simulation (left) and real system schematic (right)

The BLDC motor, as already described in previous sections, is the perfect candidate for this situation: the phase voltages may be used to recreate a speed dependent signal that can be used to obtain the sector definition just like for the hall effect sensors and consequently may be used to estimate the rotor speed, thus reducing considerably the overall cost of the system for a minor complication in hardware electronics for the acquisition of the signal and software management of the new information acquired.

The position information is obtained by exploiting the zero-crossing events, which is the moment when the phase-to-phase voltage changes its sign. It is an easy way to calculate the evolution of the rotor position and it is the reason why this kind control is so popular. The structure used to acquire the signal is different if the method is implemented on a Simulink simulation or on a real system, so the two structures are proposed in Figure 39. The Simulink block diagram is pretty straight forward, the switch block generates a square wave having a magnitude of 1 when the waveform processed is positive and 0 when the waveform is negative. The real system requires more attention and, considering the scheme presented in Figure 7 (right), the one in Figure 39 (right) is not dissimilar, the phase voltage is divided and filtered and connected to the positive input terminal of the comparator, the negative terminal is instead connected to the virtual neutral point created by using the three phase voltages, this signal is also divided and filtered in order to have a fair comparison, the output is sent to the pins of the microprocessor.

As already discussed, this technique comes with its own problems: the performance offered by the sensorless approach strongly limits the speed range the drive system is capable of covering, the load insertions and every abrupt variation of the command needs to be avoided in order to preserve smooth and protection intervention free operations, the signal conditioning needs to be improved to have a clean and reliable data source and an open loop procedure must be implemented to allow the functioning at very low speeds and the standstill start.

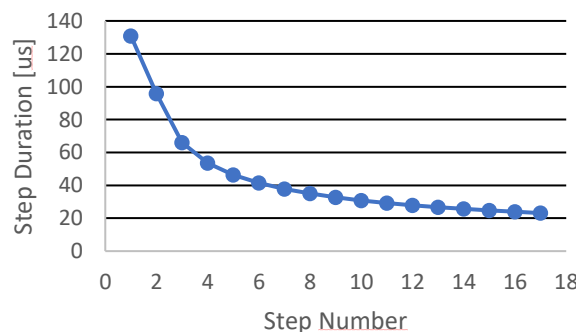


Figure 40: Graphic representation of the calculated blind steps duration

About that last problem, the start-up procedure is a requirement that can not be avoided but the lucky aspect is that it is not a complicated neither long strategy and its implementation is quick and ensure success without too much effort. As presented in the “Previous Operating Status” section a procedure

was already present and some parts were imitated from there in order to develop the algorithm of the actual start-up technique used for the work.

It is divided in two main stages, the alignment and the blind steps. The alignment consists in choosing two phases to be supplied in order to stop the rotor in one known position before the set in motion of the system, this represents a starting point for all the operations that cancels any last positioning happened before the turn-off of the system allowing to reset the configuration for the course. The blind steps are a series of open loop commands given to the motor terminals with a feedforward approach, once it is sure where the rotor is placed by the previous part, the sequence of sectors that will be energized is decided according to the rotating direction wanted. For each sector of the sequence chosen it is possible to decide both the magnitude of the voltage imposed and for how long the phases assigned to that sector would have been energized before switching to the next sector but for the strategy used in this thesis the only parameter regulated was the duration of the steps while the voltage magnitude was set to the constant value of 4.8 V to avoid exaggerated rise of the phase currents.

The blind steps duration has been calculated considering a constant acceleration regime in order to build up enough speed for the rotor to produce BEMF from whom the zero crossing events will be acquired. The calculation based on torque constant, inertia and phase current is represented in Figure 40 where the evolution of the time duration is graphically shown. Next, in Figure 41, is instead showed the start-up procedure in its entirety as it happens on the board and the stator terminals of the motor.

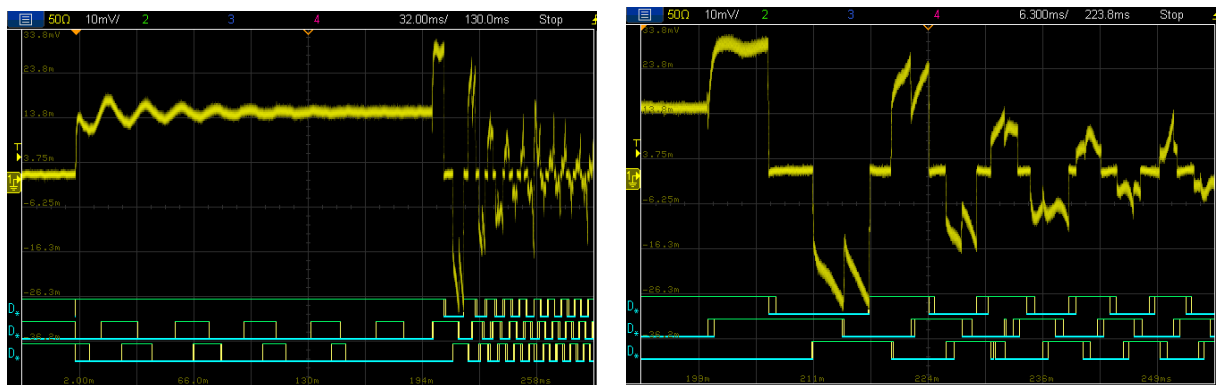


Figure 41: Start-up procedure for sensorless operations. Yellow: phase current with probe 1 A/div; Digital channels: hall effect sensors and zero-crossing event reconstruction, side to side for each phase. Alignment phase (left), blind steps (right)

On the left the alignment stage with the oscillations of the rotor, this event can be observed both from the phase current dampen fluctuation and from the hall effect sensors signal. In this section the experimental results presented will show on the same line one hall effect sensor and one signal obtained by the zero-crossing reconstruction of the BEMF, this is useful to compare the actual sensor data to the fictitious one which is used in this case. On the right the blind steps which can vary in number according to the acceleration and the overall duration of the process wanted. In this case 17 steps are used before leaving the command to the control algorithm, the decreasing magnitude of the phase current means the motor is speeding up, as can confirm the frequency of both the current and hall sensors signals. The reconstructed signal presents instead some glitches in the initial part caused by a not so perfect commutation of the phase voltages and the imprecision of the strategy at low speeds.

The presence of glitches is one important question that need to be addressed given the effects it has on the overall functioning. The principle used to build the three BEMF zero-crossing signals used as a substitution for the hall sensors is not bulletproof and its trustworthiness relies on how clean the signals used as input of the comparator are. Abrupt commutations, load insertions and any variation of the command can create false commutation events that will influence the sector definition but more importantly the speed estimation. As a matter of fact, the error in the sector definition lasts few instants, in the order of 0.1 milliseconds, and the motor inertia is capable of filtering this disturb without any problem, if it is an occasional event, but the speed estimation used as a feedback for the speed loop is way off when one of these glitches happen and a new correct value can take tens of milliseconds, too much time for the inertia too filter and more than enough to generate a chain reaction that will create more glitches until the total loss of control of the drive.

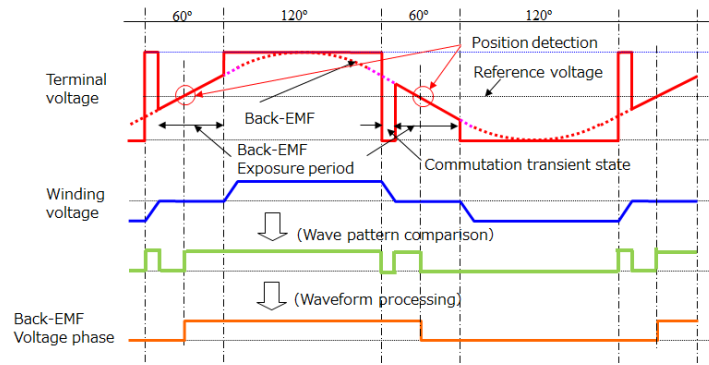


Figure 42: False commutation and glitches generation in zero-crossing detection system

The problem can be solved with a software or hardware approach: the software one is the one used by main companies like Toshiba and STMicroelectronics, the image of Figure 42 is taken from one of their application notes, it consists on the ability of their algorithms to recognize the false commutation event and discard that occurrence so to not influence the operating of the main algorithm, the hardware one, simpler and more intuitive, consists in strongly filtering the signals arriving to the comparator.

The software method requires a wide knowledge of the phenomenon, many hours of study on all the possible cases to be rejected or accepted, enough time to implement an algorithm reliable, clean and not time consuming, which leads to the other issue the computational capacity of the microprocessor needs fulfil the control loop and all the other functions in time for the update of the duty cycle. The computational power of the board is limited and in the current state it is committed for almost the 80% of the time to the satisfaction of the control requirements, moreover the software developed by those big companies benefit from years of experience and knowledge that can not be matched in few weeks of work. This is way the hardware solution was chosen, properly adjusting the components of the RC filter implemented on the board it is possible to obtain a cleaner signal and a system capable of rejecting any false commutation. This is what has been done with an analog electronic circuit simulator, the effects of different configurations have been studied to understand what solution allowed good results without too much contamination of the signal.

The drawback of using strong analog filters is in the delay this method introduces. As explained before, in some circumstances it may not be so much of a reason to worry, but in the sensorless control system the introduction of another delay may be a problem. As a matter of fact, the zero-crossing signal can be used to control the BLDC motor only considering 30 electrical degrees shift between the acquired information and the application of the new command, this is a constructive feature that can not be avoided for a correct control of the drive.

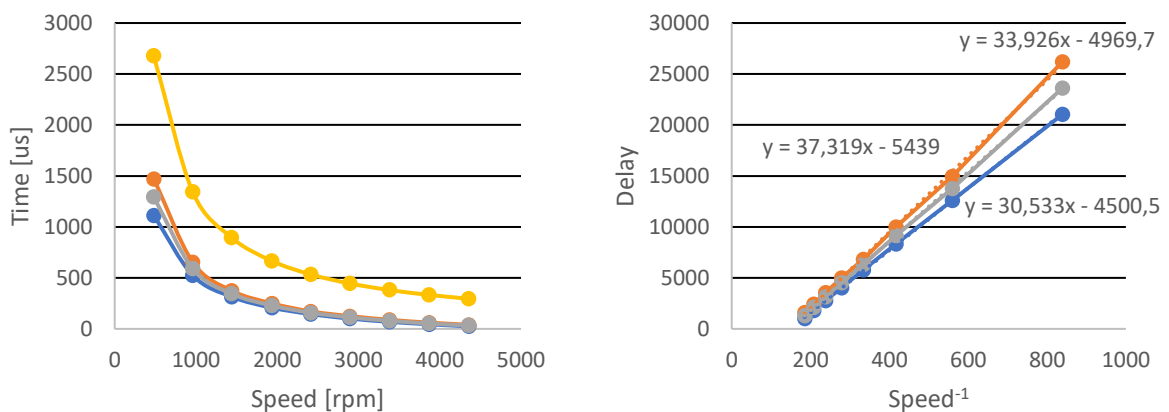


Figure 43: Excel graphics for delay compensation. Blue: rising edges phase difference, Red: falling edges phase difference, Grey: mean value, Yellow: 30°el phase difference. Time delay (left), linear interpolation for algorithm implementation (right)

So, a constant spatial delay needs to be considered every time the motor is active in sensorless operations but, the delay is not constant anymore when considering it in time intervals: it is not possible to calculate the actual space covered by the rotor but it is possible to impose to the algorithm to wait enough time to allow the motor to cover the right distance. This introduces variability and the reliance of the time delay value from the speed of the motor which is also changing during the dynamic evolution of the motion. The addition of the filter means an offset in the time delay needed for the control and, considering the delay generated by the filter depends from the frequency of the waveform that crosses it, this offset is speed dependent too.

The calculation of the time the algorithm needs to wait before updating the command must consider all of these aspects and compensate their effects to obtain a good performance. In Figure 43 are represented the graphical visualization of the computations and reflections done, the data were acquired observing the signals at constant speeds and comparing them with the values expected by theoretical considerations. On the left are shown the 30 electrical degrees curve at different speeds and the observed delay between the zero-crossing events and the hall effect sensors for rising edge, falling edge and their average value, the diagram on the right is obtained inverting the speed and calculating the value to be passed to the algorithm to apply the command correctly. It can be observed the offset between the 30° curve and the actual delays of the waveform and how this offset is not constant throughout the speed range. Inverting the diagram, it was possible to calculate by linear interpolation an equation linking the relationship between speed and needed delay, this operation was very useful for allowing correct operations and compensations of the different aspects introduced.

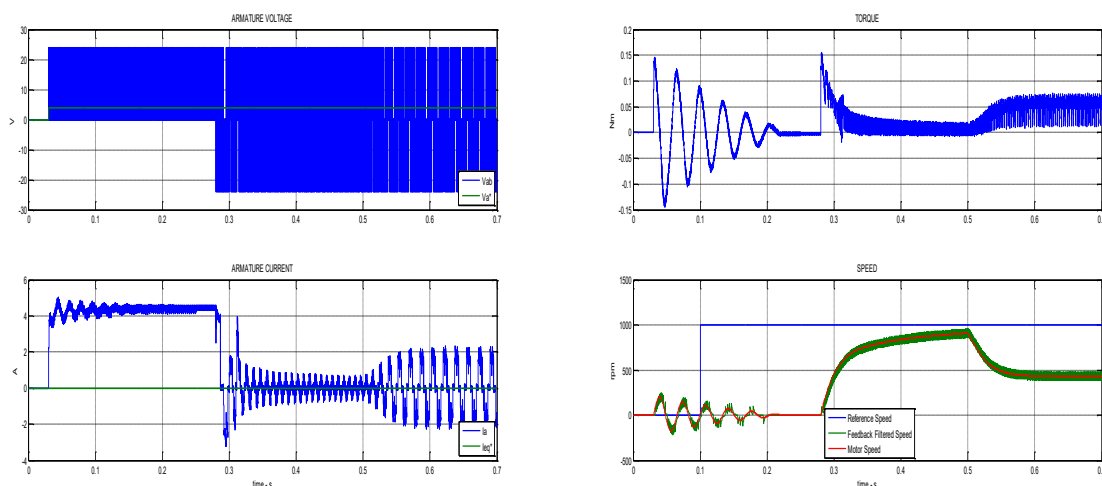


Figure 44: Open loop simulation. UP: Green, reference voltage; Blue, phase voltage, DOWN: Green, reference current; Blue, phase current (left), UP: torque; DOWN: Blue, reference speed; Red, actual speed, Green, filtered speed (right)

Just like for the sensed case, now will be showed the experimental results obtained with the Simulink and MATLAB simulation and the actual data acquired from the board. The objective was to recreate all the operative conditions previously discussed, open loop, current control and speed loop without the necessity of relying on the hall effect sensors, so the same steps have been followed to compare the results and very the goodness of the work done.

Once again, the open loop configuration used is the following:

- 1000 rpm reference speed;
- 75 Hz cut-off frequency for the speed filter;
- 0.05 Nm torque load applied at 0.5 s.

The simulation of Figure 44 clearly presents all the stages described: the alignment phase, now accompanied with mechanical information of the motor torque and rotor speed evolution with the oscillations previously explained, the start-up that smoothly accelerates the motor in few blind steps, the open loop functioning trying to speed up the motor until the reference and finally the load insertion that slows down the drive and make the phase current rise to make the motor continue spinning.

The oscilloscope screenshot displays the same stages as they happen on the real system, with the non-controlled current rising immediately after the alignment stage and then exponentially decreasing until the achievement of the regime, towards the end the load insertion requires more current and slows down the motor.

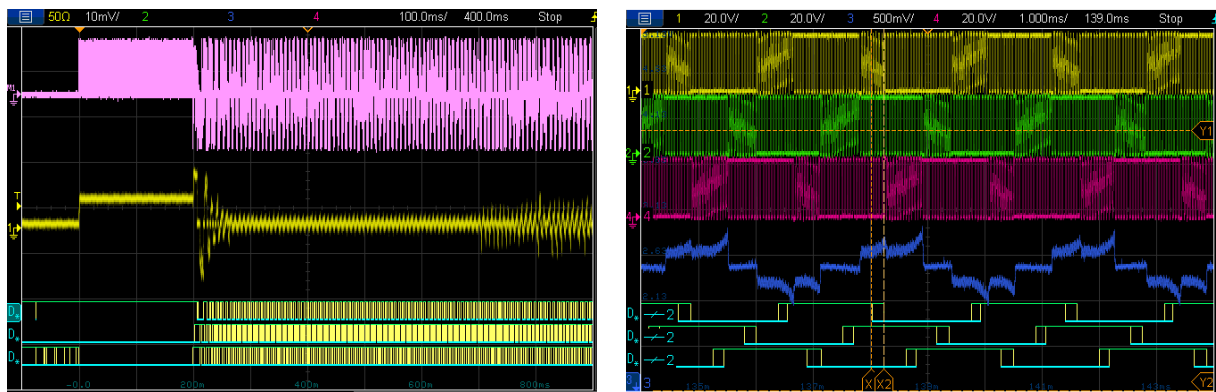


Figure 45: Oscilloscope screenshot of real system functioning. Phase-to-phase voltage, phase current with probe 2 A/div, hall effect sensors and zero-crossing event reconstruction, side to side for each phase (left). Focus on commutation delay implemented. Phase voltages, phase current with probe 1 A/div, hall effect sensors and zero-crossing event reconstruction, side to side for each phase (right)

The enlargement proposed for this situation shows how the non-controlled current evolves during the regime operations with the load connected. The absence of feedback on parameters of the drive allows the current to rise freely in each sector creating those unique waveforms. Another aspect which has been highlighted in Figure 45 (right) is the proof of the implementation of the commutation delay: the signal of the zero-crossing event starts the algorithm and in particular the timer assigned to counting the time interval requested for that particular speed, the hall sensor signal is used only to verify the goodness of the software implemented, considering the new command needs to be activated exactly in correspondence of that edge. The cursor on the image are placed to indicate one of the times the event happens but any other case is just as good. Of course the precision can not be impeccable due to the intrinsic fluctuation of the speed and the possible misalignment of the sensors other than the observed difference between the rising and falling edge's speed that forced to use an average delay value. However, even if not bulletproof, the strategy used seems to obtain the objective with enough flexibility for the purpose wanted.

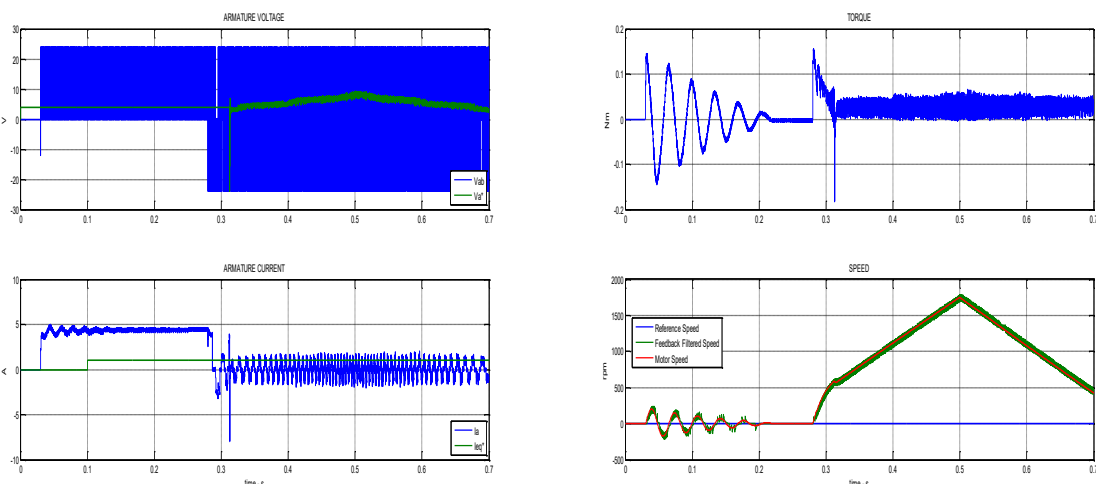


Figure 46: Current loop simulation. UP: Green, reference voltage; Blue, phase voltage, DOWN: Green, reference current; Blue, phase current (left), UP: torque; DOWN: Blue, reference speed; Red, actual speed, Green, filtered speed (right)

The current loop functioning is now presented and, as usual, the simulation is compared to the real results with the will to observe the same phenomenon and make considerations on the events. The configuration proposed is:

- 1 A reference current;
- 75 Hz cut-off frequency for the speed filter;
- 0.05 Nm torque load applied at 0.5 s.

From the simulation can be seen the speed ramp consequence of a constant torque control but the difference with the sensed case is in the initial acceleration phase. The blind steps starting stage applies a different speed rise that is clearly recognisable and the handover between the start-up procedure and the current loop control creates an abrupt change. Both the torque and current diagrams present a noticeable spike due to the sudden variation, but this is not cause of concern considering it is caused by imperfections in the computations made by the algorithm. Another main difference is in already widely discussed start-up sequence: even if imposing a low, fixed duty cycle the current involved in this stage is not fully controlled and can be much higher of the reference value of the just subsequent controlled stage. Of course the duty cycle interesting the first part was chosen in order to respect the electrical limits of the application without risking to trigger the current protections and damaging parts of the system, but for those cases in which the reference current imposed has not to be exceeded, a greater attention needs to be paid and a reduction of the duty cycle will resolve the problem.

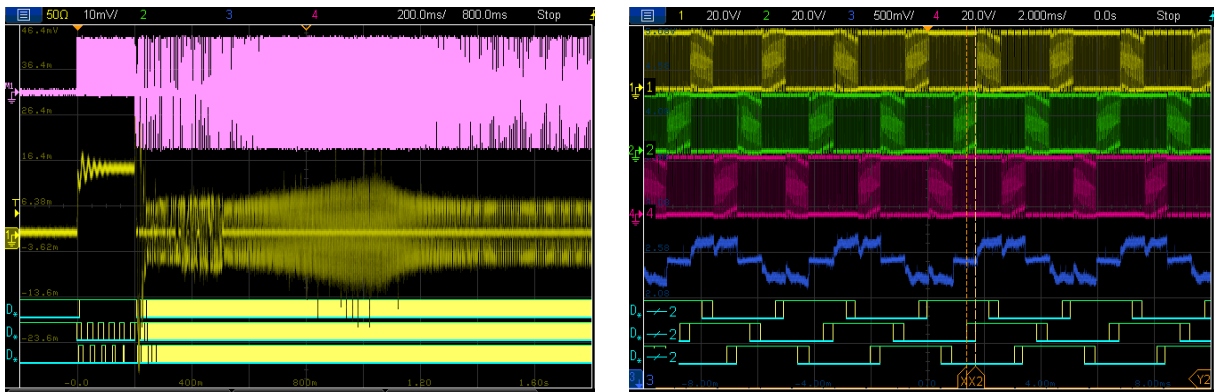


Figure 47: Oscilloscope screenshot of real system functioning. Phase-to-phase voltage, phase current with probe 1 A/div, hall effect sensors and zero-crossing event reconstruction, side to side for each phase (left). Focus on commutation delay implemented. Phase voltages, phase current with probe 2 A/div, hall effect sensors and zero-crossing event reconstruction, side to side for each phase (right)

The real system response of Figure 47 (left) proposes again the same themes, moreover the speed rise and approach to the mechanical limit of the motor makes the current noisier, out of the reference value imposed too many times, but the load insertion slows the rotor down avoiding the lost of control and bringing the phase current to its right value. The difference between the simulation and the actual system can be seen in the evolution of the phase current close to the transition from uncontrolled open loop to constant torque driven stage: if the simulation showed an unwanted current peak which created impulsive counter torque slowing down the motor, the real system struggled to engage the different routine obtaining a partially uncontrolled stage that finally converged to the usual current loop routine. This difficulty showed by the drive is due to the sudden change in the applied command, as said the sector definition obtained by the zero-crossing events, even if strongly filtered, is affected by abrupt variations generating glitches responsible of the partial loss of control.

Finally, on the right of Figure 47 can be observed again the commutation delay implemented and working with the sector sequence evolving and the algorithm correctly waiting the right amount of time to apply the new command.

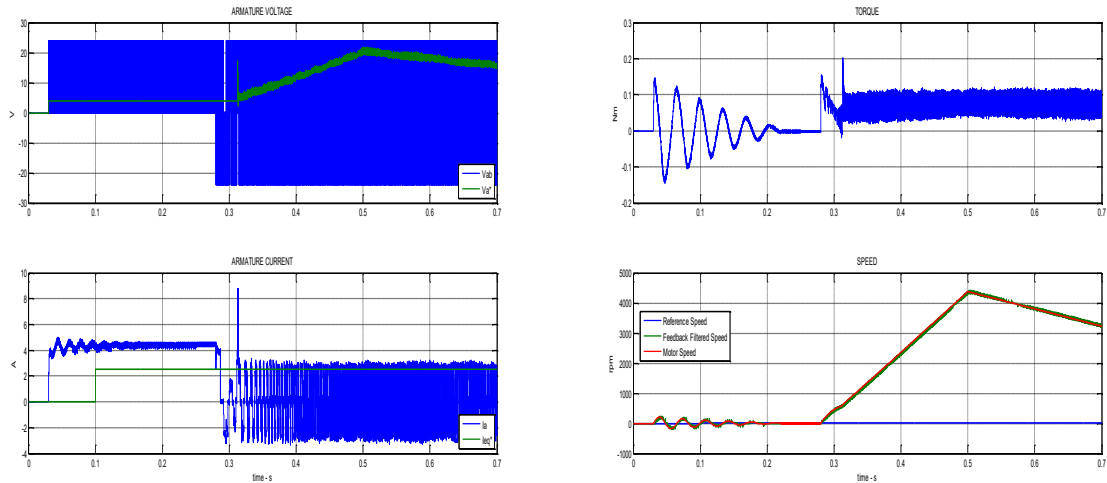


Figure 48: Current loop simulation. UP: Green, reference voltage; Blue, phase voltage, DOWN: Green, reference current; Blue, phase current (left), UP: torque; DOWN: Blue, reference speed; Red, actual speed, Green, filtered speed (right)

Just like for the examples in section 3.6 the previous results are compared with another configuration, but always for a current control loop scheme:

- 2.5 A reference current;
- 75 Hz cut-off frequency for the speed filter;
- 0.1 Nm torque load applied at 0.5 s.

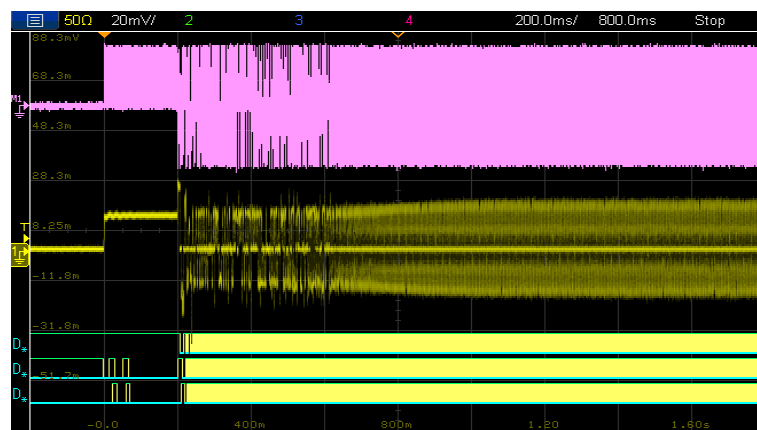


Figure 49: Oscilloscope screenshot of real system functioning. Pink: phase-to-phase voltage, Yellow: phase current with probe 2 A/div, Digital channels: hall effect sensors and zero-crossing event reconstruction, side to side for each phase.

This time the outcome is similar to the 1 A reference current, just for the reason that the max speed is not reached before the load insertion, but a different pattern can be seen in the current evolution in the oscilloscope screenshot. The simulation shows the same current spike which leads to impulsive torque and imperceptible speed fluctuations, the real system of Figure 49 instead presents the uncontrolled phase just after the blind steps sequence, the control loop converging but this time the current does not rise excessively, obtaining a better performance and a smoother evolution.

The last operative condition analysed is the speed control functioning. The objective of thought for the board was to develop a control algorithm capable of regulating the speed of the drive according to the imposed reference, for this reason the sensorless speed control is the final target to complete the work on the board and the study brought at EMA.

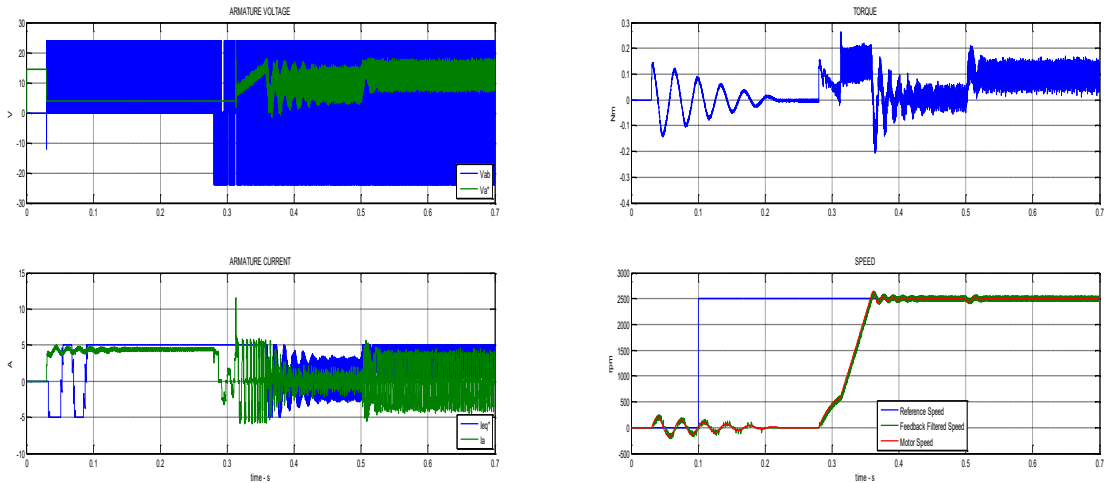


Figure 50: Speed loop simulation. UP: Green, reference voltage; Blue, phase voltage, DOWN: Green, phase current; Blue, reference current (left), UP: torque; DOWN: Blue, reference speed; Red, actual speed, Green, filtered speed (right)

In order to compare the results obtained, the configuration proposed is the same used in section 3.7 for the sensed case:

- 2500 rpm reference speed;
- 75 Hz cut-off frequency for the speed filter;
- 0.1 Nm torque load applied at 0.5 s;
- 5 A max current.

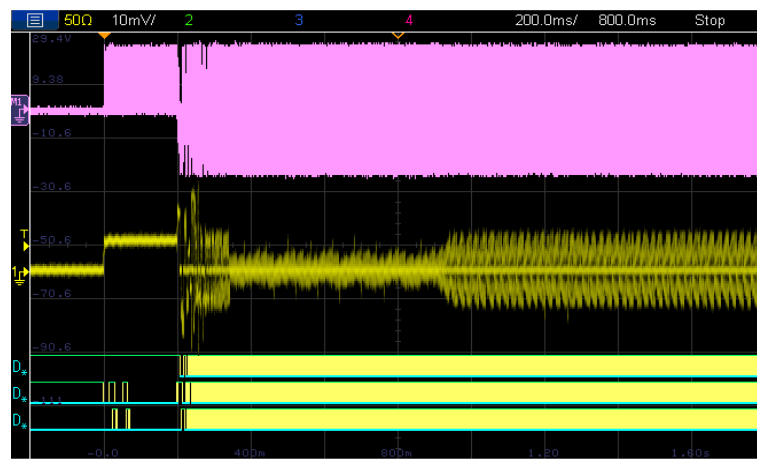


Figure 51. Oscilloscope screenshot of real system functioning. Pink: phase-to-phase voltage, Yellow: phase current with probe 2 A/div, Digital channels: hall effect sensors and zero-crossing event reconstruction, side to side for each phase.

Apart from the many times discussed start-up procedure, the simulation results are pretty similar to the sensed outcome: the speed rise, few overshoot oscillations around the reference value, regime operations without load, load insertion and deletion of the additive disturb in the chain of the block diagram. Some aspects that need attention are the difference between the speed rise in open loop functioning and speed loop control, the current spike just like the current control one, then there is the transition between the speed rise and the empty regime functioning that creates wide oscillations in both the mechanical torque and the phase current and the same happens just after the load insertion. Despite the observed oscillations, the torque evolves rapidly in the instants after the load locks in and the system is ready to respond to the sudden variation making the speed vary as little as possible.

The real system shows a new stage not used until now: just after the blind steps and before the speed loop engages the drive is commanded with an open loop technique. This is done to allow a smother transition between the different parts of the control, the open loop can intervene without any problem due to the absence of actual controlled quantities, so it can speed up the motor not worrying of the

evolution of the parameters and considering it must not start the motor from standstill, the current loss of control is not an issue this time. The duty cycle chosen for the open loop is calculated to accelerate the motor as near as possible to the actual reference speed of the subsequent control loop, so to avoid any loss of control that, considering the speed loop sensitivity, would be really difficult to recover.

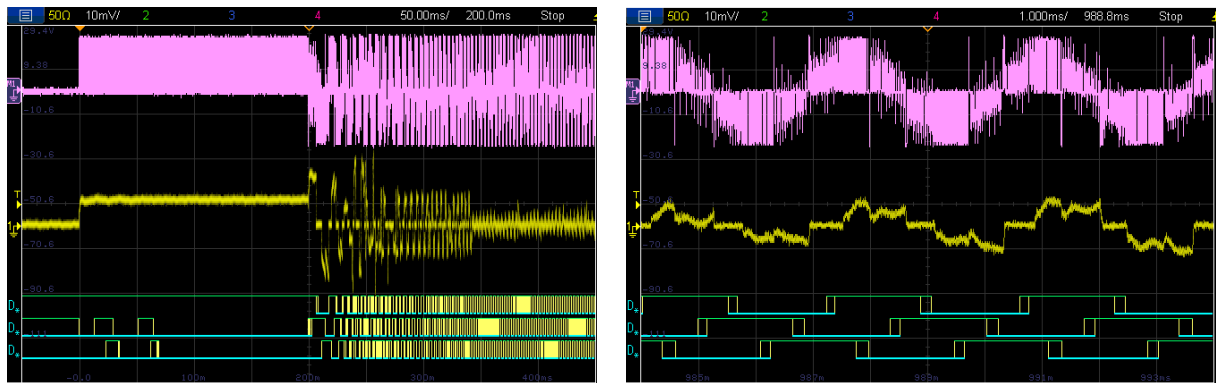


Figure 52: Oscilloscope screenshot of real system functioning. Pink: phase-to-phase voltage, Yellow: phase current with probe 2 A/div, Digital channels: hall effect sensors and zero-crossing event reconstruction, side to side for each phase. Starting sequence (left), load connected regime working (right)

The result is shown in its entirety in Figure 51 where is also possible to see the load insertion and the empty and load operations, while in Figure 52 are presented the starting sequence and the load regime enlargements with all the characteristics explained until now.

4. Future developments

The work done on the board is concluded with the implementation of the sensorless control algorithm. The steps undertaken to reach this result have shown the potentiality of the system and the wide range of applications the drive can cover without difficulties, but they also highlighted the limits and drawbacks of the main parts composing the structure.

The position loop control is one of the operations the drive can not face. The algorithm has been developed and experimented on the motor, but the results were not collected or showed due to lack on meaning. As a matter of fact, the BLDC motor, in the way it was used for this work, had the position measure discretized in 48 steps. The hall effect sensors generate 6 position pulses per electrical turn, with an 8 pole pairs structure the outcome is 48 steps per mechanical turn. This means that the distance between two consecutive steps is 7.5 degrees which is a pretty wide slice of the rotor circumference. The result of the implementation of the position loop was that the motor followed the reference perfectly when the command consisted in completing a predetermined rotation of a defined angular space but, once finished the initial movement, the rotor started oscillating around the wanted position value in a constant attempt to delete the error between the reference command and the actual position obtained. The oscillation can be more or less wide according to the magnitude of the load connected and the damping produced, but in each case the final value is not respected, especially considering that the applications requesting fine positioning need to be very precise and reliable offering high dynamic performances. One might think the solution relies on a better position sensor capable of better reconstructing and feedbacking the actual rotor position, but the problem persists due to the current ripple generated. The high dynamic request creates a positive feedback mechanism for which the position error is deleted quicker as possible overshooting the target repeatedly with an elevated torque ripple that is virtually never deleted.

One feasible improvement for the software of the drive that could also positively influence the position loop performance is the modification of the speed estimation method. One of the possibilities is to use a Phase-Locked Loop for the position and speed esteem in order to obtain a better result compared to the previous strategy used. It consisted in simply observing the time elapsed between two consecutive edges of the hall effect sensors signal and calculating the speed knowing the angular sector included between them. The PLL is a control system that generates an output signal whose phase is related to the phase of the input signal. Born as an electronic circuit, it can be software implemented with three main parts: the phase error detector, the low pass filter and Voltage Controlled Oscillator. In Figure 53 can be seen the block diagram for the PLL and its adaptation for the position estimation in the case of motor drives control.

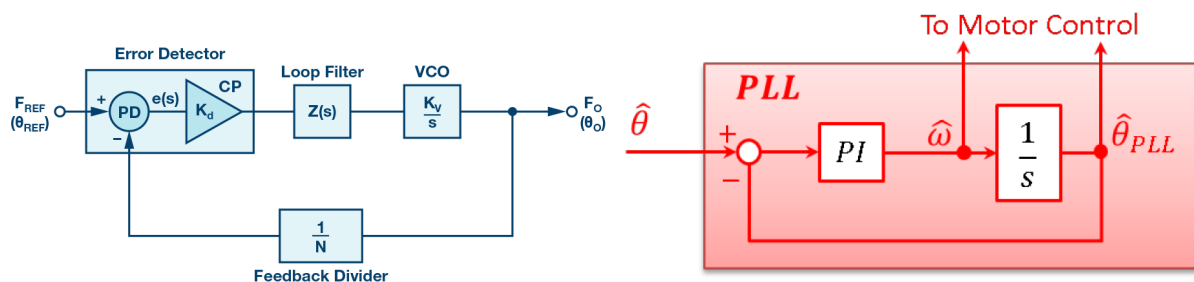


Figure 53: PLL block diagram for position estimation

The closed loop structure of the PLL tends to delete phase error between the input signal and the output signal making the estimated position closer to the actual rotor position. Another advantage in using this scheme is the possibility to extract the speed value directly from it without any other elaboration, obtaining a more accurate outcome. The system is very useful in sensorless operations when working with back-EMF signals and no actual position sensors, moreover it can be upgraded with more information provided by a position esteem from the current loop. This mechanism allows to obtain a wider bandwidth in the speed estimation routine, with good performances both in low and high speed, the downside is more complexity in developing this system and new time consuming operations for the

computational power of the board which is already overloaded, these, together with the limited time span available to develop new innovative solutions for this thesis work, are the reasons why this road was not followed.

Consequently to what just said, one hardware upgrade needed for the board is the substitution of the microprocessor. A low impact substitution was already done when the pre-existent device was changed with a new one with the only integration of one additional ADC module that would allow the simultaneous sampling of 4 more channels. This is surely a step forward in a project that aims not only to effectively control the motor drive with high performances but also to offer a user-friendly platform to interact with the parameters of the system and obtain diagnostic information. However, that is not enough when talking about implementing new feature and improving the algorithm to obtain better control and higher performances, the next step needs to be the addition of a more powerful microprocessor in terms of clock frequency, computational power and architecture in general. One of the limits is represented by the fixed-point number representation that forces to work with integers requesting a major attention to the operations involved. The use of a device with a floating-point architecture would allow higher precision and lower truncation error making also easier to develop high level firmware. The suite software already present would also benefit from this upgrade that would allow to allocate some of the power to the data acquisition and diagnostic analysis that makes of this particular board a real added value.

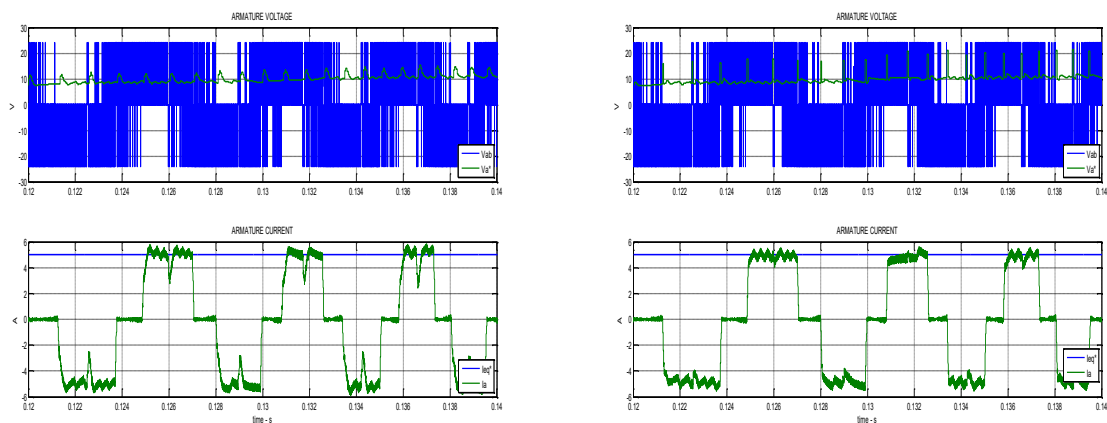


Figure 54: Feedforward command for holes elimination, before (left) and after (right) the algorithm modification. UP: Green, reference voltage; Blue, phase voltage, DOWN: Green, phase current; Blue, reference current.

One more improvement that can be done regards the holes elimination. The transition between two consecutive sectors is often abrupt and implies the modification of the phase voltages involved, this generates a delay in the current rise that needs usually 2 or 3 calculation steps before reaching the reference value. The consequence of this delay is represented by the holes in the current waveform in Figure 54 (left). The solution to this problem is very simple and allows to eliminate the delay with a feedforward command creating a smoother waveform with lower current ripple, which means lower torque ripple and oscillation in the speed of the rotor. The principle consists in giving twice the voltage used in the previous calculation step as soon as the circumference sector has changed obtaining a steeper current edge rise, thus eliminating the current holes like in Figure 54 (right). For time reasons this mechanism was implemented only on the MATLAB and Simulink simulation with optimal results, but it was not tested on the actual system where it would have requested some more experimentation.

Other upgrades thought for the application regard the power conversion stage, this is more about the purpose of the board and the size of the motor wanted. The will is to control motor with 1 kW nominal power in order to create a product able to manage different power levels and deliver the performance needed. To do so a massive renovation needs to be done and all the parts of the board must be adapted to the new power fluxes, a new set of problem may occur when managing higher performances, tracks and connectors must be able to deliver the power requested. Finally, a thermal and electrical redesign of the power conversion stage needs to be done in order to correctly exploit its characteristics and step up the performance of the whole system in optimal efficiency conditions.

Conclusions

The objective proposed for the thesis was the development of a sensorless control strategy for Brushless DC drives using the board owned by EMA s.r.l. The purpose was achieved and the work done highlighted all the positive and negative aspects of this application. Pros and cons were analysed as a preliminary step to forecast the behaviour of the system and then verified or denied during the process.

The steps followed were partially needed to achieve the final configuration, but their implementation allowed to observe the performances of the whole system, from the motor readiness and signal conditioning, to the goodness of the software created and improvement of hardware electronics. The results showed how easy and clean can be the control of a brushless motor but at the same time they exposed the limits of the application when trying to reach higher performances.

The preliminary work had a major role in the understanding of the system and improvement of the setup, here was studied the microprocessor architecture and its interaction with the signals of the board. Aspects like sampling method of the analog signals, PWM generation, management of the ISR and synchronization of all the events had a great relevance in leading the way for the algorithm creation and correct functioning. The setup was completed with hardware improvements like the substitution of the current sensors, the prototyping of the brake bench structure and the modification of small signal electronics for sampling reasons and implementation of the sensorless mechanism. While software improvements concerned the speed estimation technique, the digital filtering and the compensation of the delay introduced by zero-crossing events and analog filters.

The algorithm created consisted of four main parts: open loop control, current control, speed control and sensorless control. Easy to formulate, minimally noisy and computationally light for the board, the open loop is developed for diagnostic reasons mainly, but it also allows to impose a speed command without controlling electrical or mechanical quantities, this can be useful only in case of little and predictable load variation where there is no danger in allowing the free evolution of the electrical and mechanical parameters.

The current loop is strongly based on the machine model and it is the main character in the torque generation, it relies on the goodness of current sensors and their signal conditioning. It is used in constant load applications or when is necessary to generate a well known torque with little importance of the speed developed to move the load. It allows to control the phase currents and indirectly the motor torque maximizing performances and efficiency of the drive under monitored conditions.

The speed loop is used in applications where the reference needs to be respected independently from load magnitude, the control must cancel the error between the measured speed and the imposed one demonstrating to be insensitive to load variations, noise and any other possible disturb. The goodness of this control is based on the accuracy of the position sensor used, but they are sensitive and expensive devices, even a little constructive imprecision can generate massive fluctuations on the drive parameters.

Therefore, the option of a sensorless control is taken into account and then developed for this work. Brushless DC drives are good candidates for sensorless applications thanks to their functioning mechanisms, the possibility to eliminate the dependency from the position sensors gives to the whole system a higher reliability, eliminating problems like temperature influence on the hall effect sensors, consequences of misalignment on the speed measure, sensibility of the coupling between position sensor and rotor shaft and problems introduced by digital filtering and poor signal conditioning. The limits and drawback of this strategy were also analysed. In sensorless functioning the algorithm has to perform the same control loops as in sensed mode, that is open loop, current loop and speed loop. The software developed was capable of handling those operations as long as sudden load insertion and abrupt command variations are avoided, the speed range used is closer and the signal conditioning is strongly improved obtaining a better data acquisition for implementing the systems necessary for the correct functioning of the drive.

The overall result is positive with a great versatility offered by the drive system and the possibility to work in numerous contexts indifferently with optimal performances, the application showed also a margin of improvement that could allow to better exploit the characteristics of the system.

Figure index

Figure 1: Electrical circuit for generic three-phase power conversion stage and electric motor	2
Figure 2: Back EMF waveforms for BLDC motor and sector partitioning (left), current waveform and phase relation with the same phase BEMF (right)	4
Figure 3: Waveforms of modulation scheme, Bipolar (left), Unipolar (right). From top to bottom: carrier wave and modulating signal, gate command voltages, phase voltages, phase-to-phase voltage and moving average	6
Figure 4: Block diagram for BLDC drive control, general configuration of a position control and focus on the digital control part of the scheme	6
Figure 5: Machine control for BLDC motor, block diagram of the whole system: digital control, power conversion stage, motor and analogic data acquisition	7
Figure 6: Speed loop control block diagram, focus on the digital control system	8
Figure 7: Zero-crossing events and comparison with hall effect sensors signal (left), comparison circuit for zero-crossing detection, division and filtering on phase voltage and virtual ground (right)	9
Figure 8: Supply circuit of the board, board schematic.....	11
Figure 9: Board schematic for inverter leg, gate command circuit, shunt resistor and current sensor..	12
Figure 10: Board schematic for main signal conditioning: phase current (up left), hall effect sensor and jumper for selection of real or reconstructed signal (up right), reconstruction of position signal from back-EMF (down).....	12
Figure 11: Speed control closed loop implemented in previous software.....	14
Figure 12: Current sampling synchronization (left), events sequence of ADC sample and convert routine (right).....	15
Figure 13: Sample and convert routine on the real system. Green: phase a voltage, Blue: phase b voltage, White: phase-to-phase voltage, Yellow: phase a current, Purple: LED signal used for diagnostic, PWM interrupt and DMA Interrupt, Digital channel: ADC interrupts	16
Figure 14: Sampling and updating sequence. Note: the PWM signal is the opposite of how actually calculated on the board.....	17
Figure 15: Simulation block diagram: supply, inverter, motor and load. Input: gate commands, output: motor parameters.....	18
Figure 16: Motor parameters used for the drive control.....	18
Figure 17: Digital control block diagram, gate command generator block, inputs and outputs needed for the control.....	19
Figure 18: Under the Digital Control mask, inputs and outputs management and MATLAB S-Function block.....	19
Figure 19: Brake bench 3D printed prototype (left), electrical load connected to the dragged motor (right)	21
Figure 20: Number representation in processor architecture	21
Figure 21: Open loop control, focus on the digital control part	22
Figure 22: Open loop simulation. UP: Green, reference voltage; Blue, phase voltage, DOWN: Green, reference current; Blue, phase current (left), UP: torque; DOWN: Blue, reference speed; Red, actual speed; Green, filtered speed (right).....	23
Figure 23: Oscilloscope screenshot of real system functioning. Pink: phase-to-phase voltage, Yellow: phase current with probe 2 A/div, Digital channels: hall effect sensors	24
Figure 24: Oscilloscope screenshot of real system functioning. Pink: phase-to-phase voltage, Yellow: phase current with probe 2 A/div, Digital channels: hall effect sensors. Starting sequence (left), load connected regime working (right)	24
Figure 25: Current sensor data-sheet information on sensitivity.....	25
Figure 26: Current sensors full scale and voltage relationship, 30 A sensor (left), 5 A sensor (right) .	26
Figure 27: ADC previous functioning, the 16 pins are scanned and converted one after the other	26
Figure 28: Current loop simulation. UP: Green, reference voltage; Blue, phase voltage, DOWN: Green, reference current; Blue, phase current (left), UP: torque; DOWN: Blue, reference speed; Red, actual speed, Green, filtered speed (right).....	27

Figure 29: Oscilloscope screenshot of real system functioning. Pink: phase-to-phase voltage, Yellow: phase current with probe 1 A/div, Digital channels: hall effect sensors	27
Figure 30: Oscilloscope screenshot of real system functioning. Pink: phase-to-phase voltage, Yellow: phase current with probe 2 A/div, Digital channels: hall effect sensors. Starting sequence (left), load connected regime working (right)	28
Figure 31: Current loop simulation. UP: Green, reference voltage; Blue, phase voltage, DOWN: Green, reference current; Blue, phase current (left), UP: torque; DOWN: Blue, reference speed; Red, actual speed; Green, filtered speed (right).....	28
Figure 32: Oscilloscope screenshot of real system functioning. Pink: phase-to-phase voltage, Yellow: phase current with probe 5 A/div, Digital channels: hall effect sensors.	28
Figure 33: Oscilloscope screenshot of real system functioning. Pink: phase-to-phase voltage, Yellow: phase current with probe 5 A/div, Digital channels: hall effect sensors. Starting sequence (left), load connected regime working (right)	29
Figure 34: Misalignment. Hall effect sensors signals, position calculated starting from the signal edges (left), effect of misalignment on three speed estimation methods and corrective algorithm result.....	30
Figure 35: Speed loop simulation with 25 Hz cut-off frequency filter on the speed measure. UP: torque; DOWN: Blue, reference speed; Red, actual speed; Green, filtered speed (left). Excel reconstruction of 75 Hz cut-off frequency filter (right)	31
Figure 36: Speed loop simulation. UP: Green, reference voltage; Blue, phase voltage, DOWN: Green, phase current; Blue, reference current (left), UP: torque; DOWN: Blue, reference speed; Red, actual speed; Green, filtered speed (right).....	31
Figure 37: Oscilloscope screenshot of real system functioning. Pink: phase-to-phase voltage, Yellow: phase current with probe 2 A/div, Digital channels: hall effect sensors.	32
Figure 38: Oscilloscope screenshot of real system functioning. Pink: phase-to-phase voltage, Yellow: phase current with probe 2 A/div, Digital channels: hall effect sensors. Starting sequence (left), load connected regime working (right)	32
Figure 39: Zero-crossing detection circuit for back-EMF in simulation (left) and real system schematic (right).....	33
Figure 40: Graphic representation of the calculated blind steps duration	33
Figure 41: Start-up procedure for sensorless operations. Yellow: phase current with probe 1 A/div; Digital channels: hall effect sensors and zero-crossing event reconstruction, side to side for each phase. Alignment phase (left), blind steps (right).....	34
Figure 42: False commutation and glitches generation in zero-crossing detection system.....	35
Figure 43: Excel graphics for delay compensation. Blue: rising edges phase difference, Red: falling edges phase difference, Grey: mean value, Yellow: 30°el phase difference. Time delay (left), linear interpolation for algorithm implementation (right)	35
Figure 44: Open loop simulation. UP: Green, reference voltage; Blue, phase voltage, DOWN: Green, reference current; Blue, phase current (left), UP: torque; DOWN: Blue, reference speed; Red, actual speed, Green, filtered speed (right).....	36
Figure 45: Oscilloscope screenshot of real system functioning. Phase-to-phase voltage, phase current with probe 2 A/div, hall effect sensors and zero-crossing event reconstruction, side to side for each phase (left). Focus on commutation delay implemented. Phase voltages, phase current with probe 1 A/div, hall effect sensors and zero-crossing event reconstruction, side to side for each phase (right).....	37
Figure 46: Current loop simulation. UP: Green, reference voltage; Blue, phase voltage, DOWN: Green, reference current; Blue, phase current (left), UP: torque; DOWN: Blue, reference speed; Red, actual speed, Green, filtered speed (right).....	37
Figure 47: Oscilloscope screenshot of real system functioning. Phase-to-phase voltage, phase current with probe 1 A/div, hall effect sensors and zero-crossing event reconstruction, side to side for each phase (left). Focus on commutation delay implemented. Phase voltages, phase current with probe 2 A/div, hall effect sensors and zero-crossing event reconstruction, side to side for each phase (right)	38

Figure 48: Current loop simulation. UP: Green, reference voltage; Blue, phase voltage, DOWN: Green, reference current; Blue, phase current (left), UP: torque; DOWN: Blue, reference speed; Red, actual speed, Green, filtered speed (right).....	39
Figure 49: Oscilloscope screenshot of real system functioning. Pink: phase-to-phase voltage, Yellow: phase current with probe 2 A/div, Digital channels: hall effect sensors and zero-crossing event reconstruction, side to side for each phase.	39
Figure 50: Speed loop simulation. UP: Green, reference voltage; Blue, phase voltage, DOWN: Green, phase current; Blue, reference current (left), UP: torque; DOWN: Blue, reference speed; Red, actual speed, Green, filtered speed (right).....	40
Figure 51. Oscilloscope screenshot of real system functioning. Pink: phase-to-phase voltage, Yellow: phase current with probe 2 A/div, Digital channels: hall effect sensors and zero-crossing event reconstruction, side to side for each phase.	40
Figure 52: Oscilloscope screenshot of real system functioning. Pink: phase-to-phase voltage, Yellow: phase current with probe 2 A/div, Digital channels: hall effect sensors and zero-crossing event reconstruction, side to side for each phase. Starting sequence (left), load connected regime working (right)	41
Figure 53: PLL block diagram for position estimation	42
Figure 54: Feedforward command for holes elimination, before (left) and after (right) the algorithm modification. UP: Green, reference voltage; Blue, phase voltage, DOWN: Green, phase current; Blue, reference current.....	43

References

- [1] C.-L. Cham, Z. B. Samad, “Brushless DC Motor Electromagnetic Torque Estimation with Single-Phase Current Sensing”, J Electr Eng Technol Vol. 9, 2014
- [2] Notes from Professor M. A. Pastorelli’s course “Electrical Drives”
- [3] Notes from Professor G. Pellegrino’s course “Converters and Drives Digital Control”
- [4] A. Namboodiri, H. S. Wani, “Unipolar and Bipolar PWM Inverter”, International Journal for Innovative Research in Science & Technology | Volume 1 | Issue 7 | December 2014
- [5] J. C. Gamazo-Real, E. Vázquez-Sánchez, J. Gómez-Gil, “Position and Speed Control of Brushless DC Motors Using Sensorless Techniques and Application Trends”, www.mdpi.com/journal/sensors, 2010
- [6] “Implementation of current regulator for BLDC motor control with ST7FMC”, STMicroelectronics, AN2267, 2006
- [7] “Sensorless BLDC Motor Control and BEMF Sampling Methods with ST7MC”, STMicroelectronics, 2007
- [8] Y. Zhang, R. Ma, T. Li, Y. Xue, “Commutation point correction method of sensorless BLDC motor based on back emf detection”, IOP Conf. Series: Journal of Physics, MEIE 2018
- [9] A. Lita, M. Cheles, “Sensorless BLDC Control with Back-EMF Filtering Using a Majority Function”, Microchip Technology Inc., AN1160, 2008, 2012
- [10] “How to Power and Control Brushless DC Motors” <https://www.digikey.com/en/articles/techzone/2016/dec/how-to-power-and-control-brushless-dc-motors>
- [11] “System Design” EMA s.r.l., 2012
- [12] K. Kolano, “Calculation of the Brushless DC Motor Shaft Speed with Allowances for Incorrect Alignment of Sensors”, Metrol. Meas. Syst., Vol. XXII, 2015
- [13] “120° Square-Wave Commutation for Brushless DC Motors”, Toshiba, 2018

Acknowledgments

Un doveroso ringraziamento va alla EMA s.r.l. nella sua totalità, che mi ha accolto in un percorso di più di sei mesi, facendomi sentire parte di un gruppo forte, dinamico e motivato nello svolgere il proprio compito sempre finalizzato all'innovazione tecnologica e alla crescita personale. In particolare, ringrazio Mirko Zanotel che mi ha integrato nel suo gruppo di ingegneri e Alessandro Berruti che mi ha fornito sostegno e supporto nello svolgimento del mio lavoro attraverso difficoltà ed insegnamenti.

Ringrazio il Professor Justin Radu Bojoi che nel suo compito di insegnante è stato un simbolo di esigenza professionale e chiara visione di limiti e possibilità di crescita in tutti gli aspetti della vita, mentre nel suo ruolo di tutor ha supervisionato il mio lavoro offrendo aiuto e supporto quando necessario.

Un grazie personale va ai miei coinquilini, Carlo Ventrella e Davide Placido che nell'arco di sei anni mi hanno accompagnato in un importante viaggio di maturazione e crescita attraverso difficoltà e fatiche, lavatrici, spese, trasferimenti ma anche pizze, panzerottate in compagnia e serie tv.

Ancora grazie agli amici conosciuti a Torino e diventati parte di questa esperienza, in particolare Marco Moraschi, Luca Roggio e Marco Cascino che per comune disgrazia hanno condiviso con me il percorso universitario tra lezioni interminabili, disperazione da esame e discorsi da ingegneri spinti ai massimi livelli. E Gaetano Dilevrano e Mattia Palatresi, compagni di uscite, bevute e risate in compagnia. Grazie anche agli amici che non mi hanno abbandonato o semplicemente dimenticato quando gli eventi mi hanno portato a centinaia di chilometri di distanza.

Grazie alla mia famiglia, ai miei genitori che hanno creduto in me fin dall'inizio, senza fare domande e preoccupandosi per me nella giusta misura, nella loro consapevolezza che sarebbe stata la strada giusta per me e nella mia consapevolezza che con loro accanto ce l'avrei fatta senza problemi. E alle mie sorelle, sostegno discreto e silenzioso (o forse no) che da dietro le quinte gestisce e organizza tutto.

L'ultimo ringraziamento va ad Alice Visconti, sostegno costante, fonte di ispirazione e felicità, motivo di vita e sorgente di nuove paure e preoccupazioni, che non saranno poi così difficili da affrontare sapendo che sarai al mio fianco.